POTENTIAL ROLES OF CIRCULAR SKA3 IN EPITHELIAL OVARIAN CANCER DEVELOPMENT

OLUWATOBI AGBEDE

A THESIS SUBMITTED TO THE FACULTY OF GRADUATE STUDIES IN PARTIAL FULFILLMENT OF THE REQUIREMENTS FOR THE DEGREE OF

MASTER OF SCIENCE

GRADUATE PROGRAM IN BIOLOGY YORK UNIVERSITY
TORONTO, ONTARIO

May 2024

ABSTRACT

Ovarian cancer (OC) is the deadliest gynecologic cancer, of which epithelial ovarian cancer (EOC) is the most prevalent and aggressive form. Circular RNAs (circRNAs) have emerged as potential therapeutic targets and biomarkers in various cancers, including EOC. Our study investigated circSKA3, which was identified to be overexpressed in high-grade serous carcinoma (HGSC). Using qRT-PCR, we confirmed upregulation in HGSC tissues compared to benign and low malignant potential (LMP) tumors. Functional assays revealed circSKA3's tumor-promoting effects in HGSC cell lines, enhancing proliferation, migration, and clonogenicity. We identified its possible involvement in epithelial-mesenchymal transition (EMT) and dysregulation of cellular metabolism, contributing to increased tumor aggressiveness in HGSC. Protein pulldown assays and mass spectrometry analysis also identified potential interacting proteins. We then predicted circSKA3-miRNA-mRNA network to explore potential miRNA-mRNA crosstalk dysregulated by circSKA3 and evaluate how this might contribute to HGSC progression. Our findings suggest that circSKA3, via a complex regulatory interplay of proteins and miRNA interactions, modulates EMT and cellular metabolism to drive HGSC malignancy.

ACKNOWLEDGEMENT

To Dr Chun Peng, my supervisor, I am sincerely grateful for you taking me on, entrusting me with this project, and steering me in the right direction. Your continuous support, guidance, and motivation have pushed me to explore questions beyond my imagination and significantly piqued my research interest.

I would also like to extend my gratitude to Dr Yi. Sheng, thank you for being a member of my supervisory committee. Thank you for your helpful suggestions and support throughout this project.

I sincerely appreciate my immediate family's support, encouragement and constantly cheering me on. Thank you, Mom and Dad, for always being there and for the freedom to pursue what interests me. My brother, Ibukun, thank you for your continuous comic relief, for building Legos with me and helping me practice my presentations. You're indeed one of a kind.

I am also grateful to members of the Peng lab and my circle of friends for their unwavering support and help throughout this project.

Gagan, Riddhi, and Sajid thank you for all the humor-filled discussions, novel and movie recommendations, and for helping me with experiments when needed. You're all truly queens and kings.

Chenyang, Joyce, Yan, and Yanan, thank you for your expertise and helping me navigate protocols when I felt lost. Your assistance has been invaluable to me.

Connor, Nour, Rufei, and Sihat, thank you for helping me handle my samples and operating equipment and for sharing advice when needed. I appreciate it.

Finally, I'd like to thank everyone else who supported me in various ways throughout this project. Among them, I would like to mention Jomi, Masarath, Precious and Iyimide. Your presence, whether providing comic relief or offering a listening ear, is greatly appreciated.

TABLE OF CONTENT

LIST OF TABLES

Chapter 3

Appendix A

LIST OF FIGURES

Chapter 1

Chapter 2

Chapter 3

Chapter 5

LIST OF ABBREVIATIONS

BSJ	Back-splicing junction
CA125	Cancer antigen 125
CAF	Cystadenofibroma
CAR	Chimeric antigen receptor
CCC	Clear cell carcinoma
ceRNA	Competing endogenous RNA
circRNA	Circular RNA
ciRNA	Circular intronic RNA
CNV	Copy number variation
CRC	Colorectal cancer
ctDNA	Circulating-tumor DNA
DEG	Differentially expressed gene
DMEM	Dulbecco's modified eagle medium
EC	Endometrial carcinoma
ECAD	E-cadherin
ecircRNA	Exonic Circular RNA
ECM	Extracellular matrix
EIcircRNA	Exon-intron Circular RNA
EMT	Epithelial-mesenchymal transition
EOC	Epithelial ovarian cancer
ER	Estrogen receptor

FBS	Fetal bovine serum
FRA	Folate and folate receptor alpha
FSJ	Front splicing junctions
GCT	Granulosa cell tumors
HAS	Hyaluronan synthesases
HE4	Human Epididymis protein
HER1	Human epithelial growth factor receptor
HF	High fidelity
hnRNPs	Heterogeneous nuclear ribonucleoproteins
HYAL	Hyaluronidases
ip	Intraperitoneal
IRES	Internal ribosome entry site
LGSC	Low-grade serous carcinoma
LMP	Low malignant potential
lncRNA	Long non-coding RNA
M199	Medium 199
MC	Mucinous carcinoma
miRISC	miRNA-induced silencing complex
miRNA	Micro-RNA
MS	Mass spectrometry
NCAD	N-cadherin
NGS	Next-generation sequencing
OC	Ovarian cancer

OGCT	Ovarian germ cell tumors
OSCT	Ovarian stromal cell tumors
PARP	Poly ADP-ribose polymerase
qRT-PCR	Quantitative real-time PCR
RBP	RNA binding protein
RCC	Renal cancer carcinoma
RE	Restriction enzyme
ROMA	Risk of Malignancy Algorithm
ROUT	Robust regression and outlier removal
sc	Subcutaneous
shRNA	Short hairpin RNA
SKA	Spindle and kinetochore-associated
SLCT	Sertoli-Leydig cell tumors
SR	Serine-arginine
SRA	Sequence read archives
STIC	Serous tubal intraepithelial carcinoma
TCF	T-cell factor
TME	Tumor microenvironment
TVU	Transvaginal ultrasonography
VEGF	Vascular endothelial growth factor

CHAPTER 1

INTRODUCTION

1.1: Ovarian Cancer

1.1.1: Overview

OC is the most lethal form of gynecologic cancer, describing cancers originating from one of three anatomical sites, including ovaries, fallopian tube, and mesothelium epithelium, with most cases originating from the fallopian tube and rapidly migrating to the ovaries and surrounding regions [1]. Recent findings have also elucidated other means by which OC develops, including the development of serous and mucinous tumors into invasive cancers and an association of ovarian endometriosis with subtypes of OC[2]. OC is regarded as the "silent killer" as most cases are undetected until late stages, thus reducing patient outcomes drastically. Often, patients report experiencing no symptoms in the early stages and only present with unsuspecting symptoms such as abdominal bloating, pelvic pain, frequent urination, and increased feelings of satiety at later stages. However, as these symptoms are primarily associated with numerous diseases, including stress, patients are unlikely to report this to their clinician and test for OC[3]. Furthermore, current detection methods are limited in their sensitivity and specificity, as levels of current biomarkers, CA125 and HE4, vary widely across patients for different reasons. Primary OC treatment involves an aggressive platinum-based chemotherapy regimen with surgical debulking pre- or post-chemo, and in more severe cases, patients are managed to reduce their level of discomfort[4]. These treatment methods lessen the patient's quality of life and are often followed by more aggressive and resistant relapse in about 80% of patients with advanced-stage OC[4]. Considering the challenges posed with detecting and treating OC, it's also imperative to recognize the various risk factors associated with its incidence, including genetic, hormonal, reproductive, and social factors, with a family history of OC being the most crucial predisposing

factor[5]. Ultimately, a better understanding of OC biology is essential to improve patient outcomes.

1.1.2: Types of OC

The ovaries have numerous cell types, including epithelial, germ, and stromal cells. These are possible sources of OC with an approximate incidence of 90%, 3%, and 2%, respectively, and other non-specific cases being 5%[6].

1.1.2A: Epithelial Ovarian Cancer

EOC is a heterogeneous disease, formed from the transformation of epithelium cells of the ovary into malignant tumors and vastly classified into serous (High grade and Low grade), endometrial, clear cell, and mucinous carcinoma with approximate incidences of 75%, 5%, 10%, 7%, and 3% respectively.

1.1.2A.I: High-Grade Serous Carcinoma

HGSC is the most prevalent subtype of EOC originating from serous tubal intraepithelial carcinoma (STIC lesions); thus, they share morphological and genetic characteristics. Histopathologically, HGSC resembles a solid mass of cells with slit-like perforations and papillary or glandular structures resembling the epithelium of a fallopian tube. At a cellular level, they present with high-grade nuclear atypia (hyperchromatic with increased variation in size and shape), high mitotic index and abundance of mitotic cells (indicative of increased cellular division), and psammoma bodies[7]. Immunohistochemical markers, including *P53, WT1, CDKN2D, CK7, ARID1A,* and *PAX8,* differentiate HGSC from other EOC or similarly presenting tumors[8]. Severe genomic instability also characterizes HGSC; a large TCGA study identified prominent mutations such *as BRCA1/2, CSMD3, NF1, CDK12, GABRA6, RB1*, and, more frequently, high copy number variation (CNV) of *CCNE1*, *MYC*, and *MECOM*.

Furthermore, major tumor suppressor genes, including *PTEN, RB1*, and *NF1*, were homozygously deleted in some HGSC[9]. Inter-chromosomal fusion of *CDKN2D-WDFY2* genes has also been reported in some cases of HGSC and constitutionally activates the PI3-AKT pathway, contributing to HGSC development[10]. High-grade tumors resist etoposide and doxorubicin and are more susceptible to paclitaxel and carboplatin treatment [11].

1.1.2A.II: Low-Grade Serous Carcinoma (LGSC)

LGSC is a subtype of EOC with a distinct molecular and genetic profile. They are more genetically stable and less invasive than HGSC and typically resemble tumors of LMP as they are derived from this precursor state. They are often tubal, mostly originating from the fallopian tubes and, in rare cases, from tubal epithelium outside the fallopian tube arising from endosalpingiosis[12]. Morphologically, they present as a relatively uniform cell population with varying architecture (including cuboidal, low columnar, or flattened), mild cellular atypia, uniform chromatin distribution, low mitotic index, and presence of psammoma bodies and or mucin. Primarily, their structure resembles a normal cell more than HGSC's; however, LGSC could also be associated with HGSC at presentation or following recurrence[13]. The genetic landscape of LGSC from different genomic and immunohistochemical studies reveals an increased mutation in *KRAS, BRAF, NRAS, PIK3CA,* and *USP9X*[14,15], suggesting a crucial role of the MAPK and RAS/RAF pathway in their development and further confirms their origin as the fallopian tube epithelium[16]. LGSC patients are typically younger and resist paclitaxel and carboplatin drugs, while they are more susceptible to etoposide and doxorubicin-based treatment[11].

1.1.2A.III: Endometrial Carcinoma (EC)

EC is another type of EOC originating from the endometrium following endometriosis, lynch syndrome[17,] or endometrioid borderline tumor leading to endometrial hyperplasia[12]. They appear as well to moderately differentiated adenocarcinoma, often resembling normal cells of the endometrium. They are characterized by the budding of tumor cells, cytological atypia, psammoma, and slit or round spaces[8,18]. EC commonly possesses genetic mutations in *TEN, CTNNB1, PIK3CA, KMT2D, KMT2B, PIK3R1, ARID1A,* and *TP53* and widespread CNV. This hypermutation is explained by the mutation of *POLE* gene and a deficiency in the mismatch repair pathway[19]. Surgery is commonly used as the primary treatment method for EC, followed by adjuvant treatment using radiotherapy and or platinum-based chemotherapy drugs for effective management of EC [20].

1.1.2A.IV: Clear Cell Carcinoma (CCC)

CCC is a type of EOC presenting as glycogen and lipid-containing clear cells in the ovaries and surrounding organs. Atypical endometriosis and clear cell adenofibromas have been constantly reported as a precursor to CCC. Visually, they appear as a combination of papillary, tubulocystic, and solid growth patterns with a clear cytoplasm[21]. A background of endometriosis and hyalinated stroma further distinguishes CCC from HGSC and EC. Distinct immunohistochemical staining patterns include the presence of *HNF1-B* and napsin A and are negative for Wilms tumor 1 and estrogen receptor (ER)[22]. They often present with similar mutations as in EC with increased prevalence of *ARID1A, PIK3CA, PTEN, and MS1* mutations[12], suggesting a role of the SWI/SNF chromatin remodelling complex, MAPK, and PI3K/AKT pathways in CCC development and progression[21]. Although genetically stable, notable CNV, including a gain of *ZNF21*(a potential sign of PI3-AKT activation) and deletion of tumor

suppressors such as *RB1* and *TP53*, have also been reported in CCC and might contribute to tumorigenicity[22]. CCC also shows resistance to platinum-based treatment and thus relies on pathway-specific (such as mTOR and VEGF, among others) therapeutic targets and various surgeries for treatment [23].

1.1.2A.V: Mucinous Carcinoma (MC)

MC is the least occurring subtype of EOC with a more favorable prognosis and numerous origins, including germ cells, ovarian teratomas, and metaplasia[24]. Due to the absence of distinct origins, they are morphologically heterogeneous but generally possess papillary and cystic masses containing mucinous fluid[12]. They are often regarded as a separate disease entity as their genetic profile differs from most EOC. Their growth stems from the slow progression of mucinous borderline tumor into invasive carcinoma and is characterized by mutations in *KRAS, HER2, BRAF, TP53, ERBB2, APC,* and *CTNNB1* genes[24]. Unlike other EOCs, tobacco smoking is the primary risk factor associated with MC[25]. Treatment methods currently rely on surgery (surgical or cytoreductive, dependent on the stage). They are also usually followed by platinum-based chemotherapy due to their low resistance.

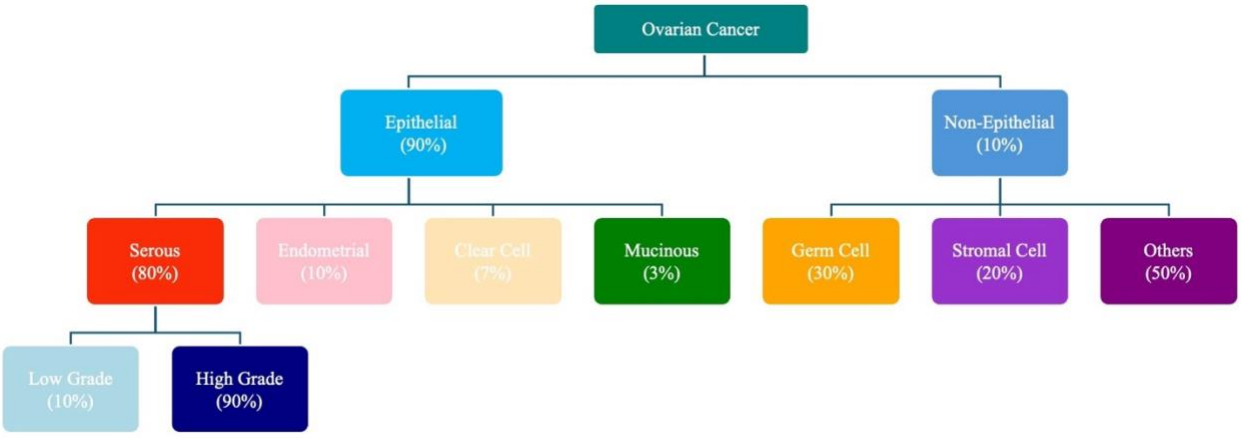

Figure 1.1: Summary classification of OC subtypes and their approximate incidence

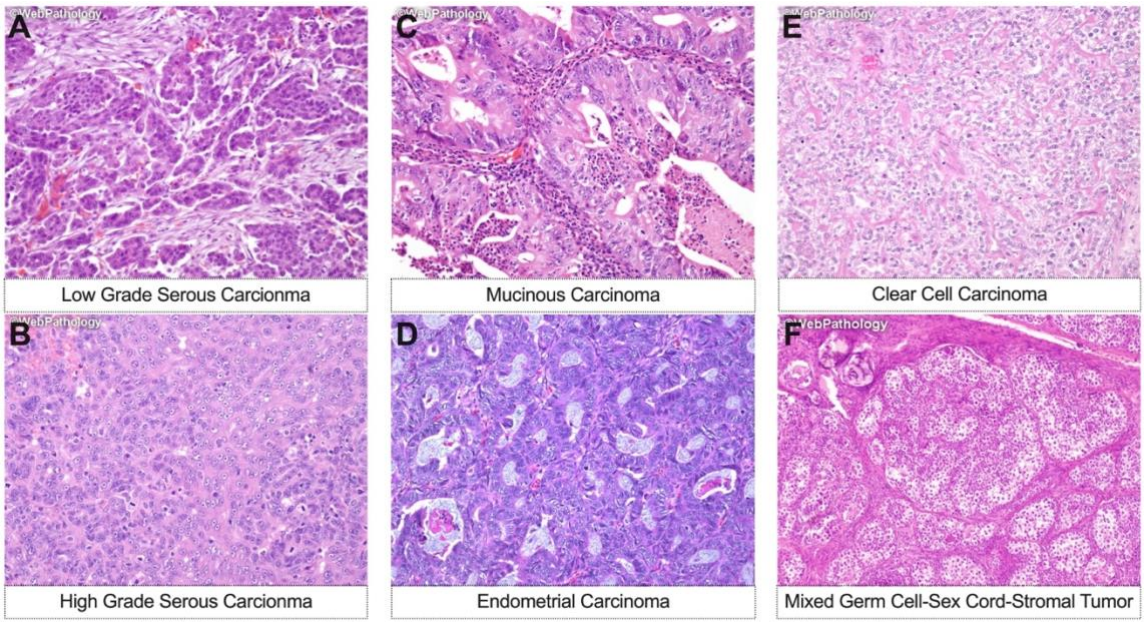

Figure 1.2: Representative histological images depicting various types of EOC.

Low grade (A), high grade (B), mucinous (C), endometrial (D), clear cell carcinoma (E), and mixed germ cell-sex cord-stromal tumors. Obtained with permission from WebPathology[26].

1.1.2.B: Ovarian Germ Cell Tumors (OGCT)

OGCT is rare (3%) and occurs in teenage girls and young women. They present with heterogeneous patterns originating from primordial germ cells and sex stromal cells. They are

widely subdivided into dysgerminoma, which refers to germ cell tumors originating from the ovary, and non-dysgerminomas with mixed origins, including teratomas and yolk sac tumors. More specifically, they are classified into three major groups by the WHO, including cells of primitive origin, biphasic or triphasic teratoma, and monodermal teratomas[27,28]. OGCT presents as large tumors and occasionally has a cystic component. Positive staining for pluripotency markers such as *OCT3/4, SALL4, NANOG, LIN28, PLAP, CD-117,* and *D2-40* is also observed in OGCT[29]. Genetic studies indicate an overall low mutation rate, frequent mutation of the *KIT* gene, and increased CNV in parts of chromosome 12 across germ cell tumors[30].

1.1.2C: Ovarian Stromal Cell Tumors (OSCT)

OSCT is the most uncommon (2%) ovary neoplasm. Pathologically, they are unilateral with polymorphism across the different subtypes, including granulosa cell tumors (GCT), Sertoli-Leydig cell tumors (SLCT), sex cord tumors, and mixed forms[31]. Briefly, GCT originates from sex-cord stromal and is present in juveniles and adults, often exhibiting hormonal symptoms such as hirsutism, virilization, and precocious puberty. They are characterized by Sertoli and Leydig cells in the ovaries[8]. *DICER1, STK11,* and *FOX2* mutations are prevalent across the different subtypes of OSCT and contribute to their tumorigenesis[31].

1.1.3: Stages of EOC

5-year relative survival rates of EOC patients drastically decrease from approximately 90% in stage I to 20% in stage IV[32]. Stages are marked by a gradual progression of the tumor from being limited to the ovaries (Stage I) to an extension to the pelvic regions (Stage II), followed by advancement to abdominal and pelvic peritoneum (Stage III) and then distant metastasis (up to the liver and spleen) at the final stage[33]. EOC Progression is categorized using the FIGO staging system, focusing on the size of the primary tumor (T), the extent of immediate

lymph node metastasis (N), and distant metastasis (M). Briefly, FIGO describes the size of the primary tumor from T0 to T4, indicating the presence of no tumor at T0, confinement to the ovaries and fallopian tubes at T1, pelvic extension at T2, microscopic peritoneal metastasis at T3 and prominent distant metastasis at T4. N and M classifications are simplified as 0 and 1, representing absence and presence, respectively. Following the FIGO system, EOC progression is classified into four stages (I to IV) indicative of overall tumor metastasis and prognosis[34].

At stage I, the tumor is confined to the ovaries with no metastasis or lymph node involvement. Typically, progression begins from one ovary or fallopian tube only at Stage IA and then into both ovaries or fallopian tubes at Stage IB. In cases where surgical spills occur, tumor rupture happens, or tumors are observed on the surface of the ovary or fallopian tubes, or malignant cells are detected in the ascites fluid, EOC progresses to stage IC. This categorizes the end of stage I and precedes stage 2[34]. At this stage, the five-year cause-specific survival rate is about 89%[35].

Following the pelvic extension, the tumor advances to stage 2. Specifically, extensions to the uterus and/or ovaries and/or fallopian tubes mark stage IIA, followed by further extension into the pelvic intraperitoneal tissues in stage IIB[34]. At this stage, the five-year cause-specific survival rate is about 71%[35].

By stage 3, the tumor has now spread to the peritoneum on the pelvis exterior and may include metastasis to the associated lymph nodes. This progression follows a stepwise pattern beginning with confirmed retroperitoneal lymph node metastasis in stage IIIA into small, microscopic (up to 2cm) extra pelvic metastasis in stage IIIB. Afterward, the tumor enlarges by stage IIIC into macroscopic (>2cm) extraperitoneal metastatic cells[34]. At this stage, the 5-year

cause-specific survival rate stands at approximately 41%, reflecting a slightly favorable outcome[35].

At the most advanced stage, the tumor metastasizes beyond the peritoneal. Pleural effusion indicating metastasis to the lung marks stage IVA and is often followed by rapid progression to the parenchyma, extra-abdominal tissues, and lymph by stage IVB[43]. Case-specific survival and patient outcomes at this stage are meager at approximately 20%[35].

1.1.4: Detection Methods

Currently, diagnosis of EOC is limited to the use of cancer antigen 125 (CA125), human epididymis protein (HE4), risk of malignancy algorithm (ROMA), and transvaginal ultrasonography (TVU). However, concerns regarding sensitivity, specificity, and invasiveness exist for all these diagnostic modalities.

CA125, a leading serum biomarker of EOC, is often preferred by patients as detection is less invasive than TVU. However, high false positive rates with less than 80% sensitivity and specificity are associated with it[36]. This is primarily due to the fluctuation in CA125 levels related to multiple factors, including menopausal status (with higher levels in premenopausal women), race (higher levels in Caucasians), pregnancy, and serious physiological disorders like heart failure[37]. Moreover, in the context of early-stage OC, CA125 may not consistently manifest at detectable levels[38].

HE4 is another serum biomarker that reportedly holds greater potential in detecting EOC, with its detection being exclusive to EOC patients and, in rare cases, other gynecologic tumors. Level of tumor differentiation, tendency for recurrence, and chemotherapy sensitivity also appear to be associated with HE4 expression. For instance, HGSC exhibits HE4 expression in 100% of cases, whereas LGSC shows HE4 expression in 79%. Unlike CA125, HE4 levels are relatively

stable and unaffected by hormonal fluctuations (e.g., menstrual cycle). While the increased sensitivity and specificity of HE4 in detecting both early and late-stage OC make it more desirable compared to CA125 in certain contexts, it is important to note that extensive clinical validation is still ongoing[39,40].

ROMA implements a mathematical formula combining CA125 and HE4 levels and adjusts for the patient's menopausal status to detect OC. Following the calculation, patients are numerically categorized as low to high risk, which informs the treatment approach and avoids unnecessary invasive tests and surgery. As a detection tool, it is advantageous as it is more sensitive and specific than individual serum biomarkers alone. Despite promising results, continued validation using diverse patient cohorts is still required to assess the generalizability and reliability of ROMA[40].

TVU is another detection method widely used due to its relative effectiveness in the early detection of EOC. It is the only imaging technique for EOC detection and involves the insertion of an ultrasound probe into the vagina to obtain high-resolution images of the ovaries. A physician's physical assessment of the image is then carried out to identify irregularities in the ovaries. Limitations to using TVU as a primary diagnostic tool lie in its relative invasiveness, technical difficulties, and inability to distinguish between different types of tumors. Clinicians often combine TVU with ROMA to obtain a more complete report for detecting and developing a treatment course for EOC[41].

1.1.5: Risk Factors

The current diagnostic landscape for EOC presents opportunities and challenges as they offer varying degrees of sensitivity, specificity, and invasiveness. Elucidating the intricate

interplay between genetic, environmental, and lifestyle factors as potential risk determinants is promising for advancing EOC prevention and early detection strategies.

Genetics plays the most crucial role in predisposing an individual to EOC. Numerous studies have reported an association between the chances of developing EOC and levels of mutation in tumor suppressor genes and *BRCA1/2* germline mutation. Furthermore, a family history of EOC or other gynecologic cancers further increases patients' disposition to EOC[9].

Reproductive events and associated physiological mechanisms can predispose individuals to EOC. According to the incessant ovulation theory, heightened ovulatory cycles lead to repeated tissue tearing in ovarian epithelia, necessitating more frequent repair processes. This continual repair could also increase the likelihood of developing EOC[42,43].

Hormonal levels also influence the risk of developing EOC, as research suggests that prolonged exposure to fertility treatments may elevate the likelihood of EOC development. Conversely, a higher frequency of hormonal contraceptive pill usage is linked to a reduced EOC risk. These observations, though intensely debated, align with the principles of the incessant ovulation theory. This theory posits that the significant increase in ovulation associated with fertility treatments and the decrease observed during hormonal contraceptive use may correlate with alterations in EOC risk[42,43].

Various lifestyle factors, such as dietary habits[44], physical activity levels[45], socioeconomic status[46], and alcohol and tobacco consumption[47], have also been suggested to influence an individual's susceptibility to EOC. While studies present varying correlations between these factors and EOC risk, adopting a healthier lifestyle may mitigate the predisposition to EOC or improve prognosis.

1.1.6: Current Treatment Methods

Effective treatment and management plans can be developed depending on the stage and subtype of EOC detected. Surgical resection of the affected region is the default method of treating EOC. This is usually followed by adjuvant chemotherapy treatment to prevent future development of cancer cells. In cases where surgical resection is impossible or difficult, chemotherapy could be used before and after surgery to shrink the tumor size, increase surgical success, and prevent further growth of cancerous cells [48]. Major concerns of this treatment regimen include the toxicity of chemotherapy to the cells, as intense cycles of chemotherapy (between 3-6 complete cycles, depending on the cancer stage) are needed to manage EOC. Proof from the relative survival rate shows that treatment vastly increases patient survival in early-stage cancer. However, due to the subtle nature and the quick prognosis of OC, most cancer patients are left undiagnosed until the late stages, thus reducing the treatment effectiveness drastically. In most cases, patients in the late stages are subjected to management therapy as treatment offers little to no help to the patient [49].

Scientists have turned to a personalized medicine approach as an alternative to traditional treatment methods. This involves the development of targeted therapies designed to alter abnormal cellular pathways associated with cancerous cell development in the patient. This treatment field is considered revolutionary as it promises effective treatment with minimal toxicity and optimum quality of life for patients. Some of these techniques include pathway inhibitors, immunotherapy, and antiangiogenic agents. Promising pathways currently exploited in targeted therapies include the Vascular Endothelial Growth Factor (VEGF), Poly ADP-ribose polymerase (PARP), folate and folate receptor alpha (FRA), Human Epithelial Growth Factor Receptor (HER1) and Chimeric Antigen Receptor (CAR) T cell therapy, amidst others [50,51].

As it is essential to detect EOC early and increase the effectiveness of treatment, current works are actively exploring more sensitive, specific, and less invasive detection and potential therapeutics methods, including using biomarkers such as long non-coding RNA (lncRNA), circulating-tumor DNA (ctDNA), mRNA, and circular RNA (circRNA)[52]. The concept behind these involves an effort to regulate the growth pathway of cancerous cells, aiming to restore regular cellular mechanisms, and it is promising in improving patient outcomes and reducing the likelihood of relapse, which sometimes occurs in patients due to chemotherapy resistance.

1.2: Circular RNA

1.2.1: Overview of Circular RNA

circRNA denotes a subclass of RNA molecules generated through back-splicing events of pre-mRNA, characterized by a unique ring-like RNA structure achieved through the covalent connection between its 3’ and 5’ ends, thus forming a distinctive back-splicing junction (BSJ)[53]. Their biogenesis relies on a downstream splice-donor site and an upstream splice-acceptor site. Complementary repeats or protein binding sequences flank these splice sites to aid the ends' covalent linkage. Like alternative splicing in linear RNA, back-splicing events in circRNA can produce different combinations of exons and introns in the final circRNA product. These include the exonic (ecircRNA), circular intronic (ciRNA), and exon-intron (EIcircRNA), consisting of exons only, introns only, and exon-intron, respectively[54]. ecircRNA, the most abundant type of circRNA, primarily localizes within the cytoplasm, while the other types are found in the nucleus[55]. circRNAs are more stable than their linear counterparts as they are less susceptible to exonuclease degradation due to a lack of poly-A tail and G cap modifications. Their increased stability makes them desirable as potential therapeutic targets and biomarkers. Current findings pose three significant functions of circRNA: micro-RNA (miRNA) sponging, transcriptional

regulation, and protein binding. Consequently, understanding circRNA biogenesis, mechanisms of action, and their functional implications has become crucial for exploring novel therapeutic avenues across different complications[24].

1.2.2: Biogenesis

The biogenesis of circRNA relies largely on back-splicing events. Despite their increased stability, cellular processes facilitate the production of linear RNA over the circular form, as observed by their increased endogenous abundance. This suggests that back splicing, as a process, might be unfavorable or more complex, possibly from a spliceosome assembly point of view. As such, RNA circularization is mainly reliant on the presence of cis-elements (including intronic complementary sequences and repetitive flanking sequences) and trans factors (including RNA binding protein (RBP), splicing factors, and heterogeneous nuclear ribonucleoproteins (hnRNPs))[56]. Supported by evidence from numerous studies, RNA circularization is facilitated by complementary flanking sequences and repetitive *Alu* elements. RBPs promote circularization by one of two primary mechanisms: RBPs like MBPL1 and QKI[57] bridge two flanking introns together, and others like ADAR1 act via their dsRNA binding activity. Splicing factors such as serine-arginine (SR) proteins and hnRNPs also contribute to the circularization of RNA, often acting in a combinatorial manner to produce circular RNAs using their intronic sequence[58]. After either of these circularization processes, intronic regions could be retained or spliced out to form EIciRNA or ecircRNA, respectively. Also notable is the exon-skipping during pre-mRNA processing, driving the formation of a lariat. This is followed by an internal splicing process during which ecircRNA, or EIciRNA, is produced. ciRNAs are rare as their formation relies on producing an intact removed-intron-containing lariat. These lariats are only preserved with 7 nt GU-rich elements near the 5’ splice site and 11 nt C-rich elements near

the branch point; otherwise, they are debranched and degraded[55]. Alternative circularization also occurs in these RNAs, allowing the formation of multiple circRNA from a single gene locus with different combinations of introns and exons included or excluded[56].

1.2.3: Functions

circRNAs mostly function as miRNA sponges, capable of binding to miRNAs and preventing them from interacting with their target genes to reduce their expression level. One circRNA can often interact with multiple miRNAs through complementary binding sequences[59]. They can also interact with proteins by acting as protein decoys (mimicking proteins to interfere with the normal signalling pathway in the cell competitively) or protein scaffolds (facilitating the assembly of protein complexes). Through this, they can regulate biological processes, including cellular proliferation, tumor suppression, and cell cycle progression[59].

In rare cases, circRNAs can also be translated into peptides. This is facilitated by the presence of an internal ribosome entry site (IRES) or modification of adenosine to form N^6-methyladenosine. In this capacity, they can act like other peptide molecules and regulate cellular processes[59]. Nuclear-located circRNA, including EIcircRNAs and ciRNAs, have also been reported to contribute to host-gene transcription by interacting with RNA polymerase and the spliceosome complex[60].

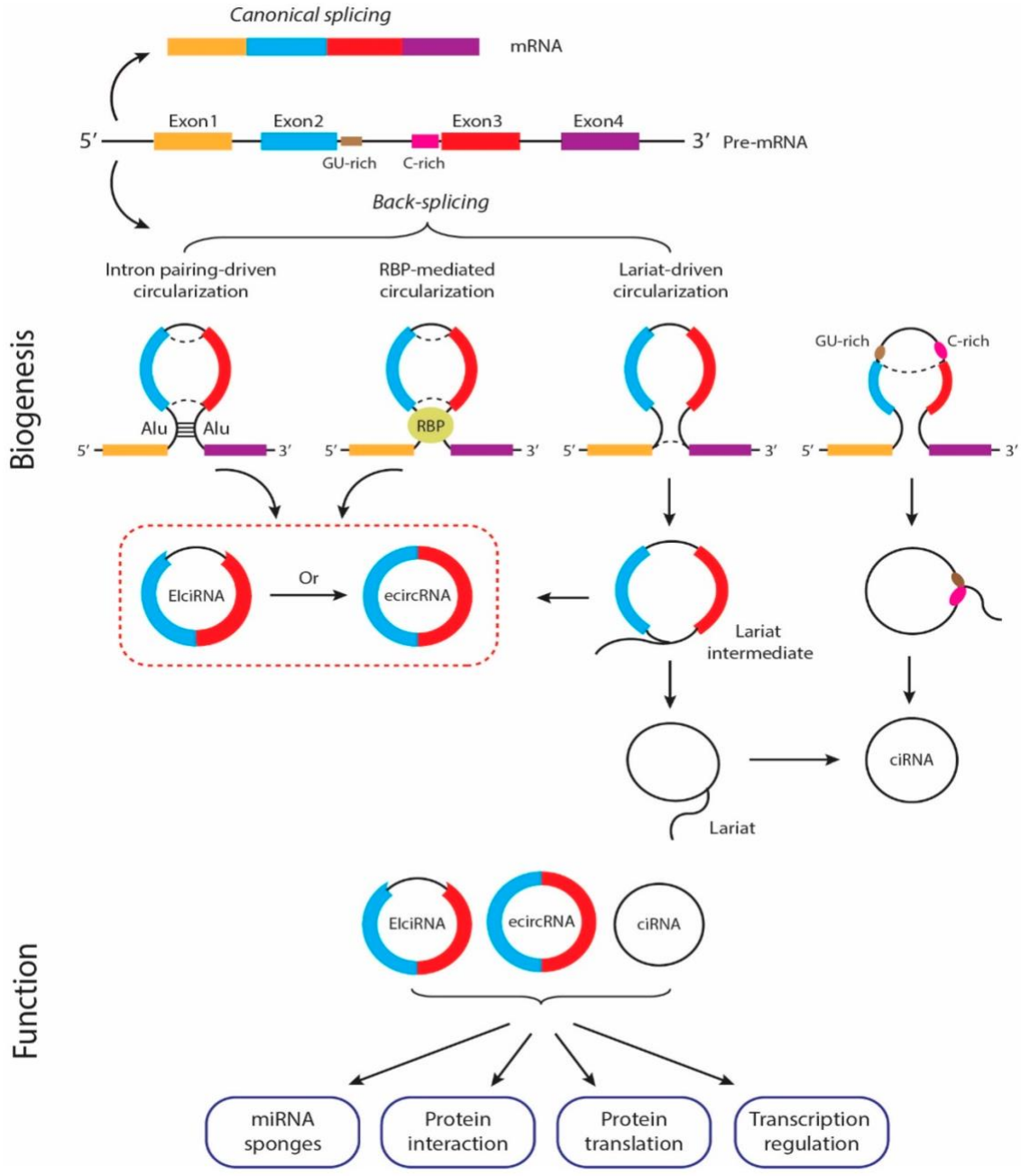

Figure 1.3: Summarized schematics of circular RNA biogenesis from mRNA and their reported modes of action.

circRNA is formed through back-splicing events of pre-mRNA, resulting in a ring-like RNA structure. Mechanisms of circularization involve cis-elements, trans factors, and alternative circularization processes, influencing the formation of various circRNAs. They also serve multiple functions, such as miRNA sponging, transcriptional regulation, and protein binding. Obtained with permission from Qiu et al.[24]

1.2.4: Role of circRNAs in EOC development

With the advent of integrative bioinformatic research, circRNAs and their contribution to the development of cancers, including EOC, are increasingly recognized. While most circRNAs exert tumor-promoting effects in EOC, tumor-suppressing abilities have also been reported in EOC. More recently, circATP2B4 was reported to be overexpressed in EOC tissues, correlated with tumor progression, and found to promote tumor progression and metastasis by inducing macrophage polarization via miR-532-3p sponging[61]. Similarly, hsa_circ_0007615 was found to be significantly overexpressed in EOC tissues and cell lines, and tumor-promoting activities of the cells were blocked upon knockdown. Rescue experiments with miR-874-3p abolished the blocked tumor-promoting activities, suggesting miR-874-3p sponging and modulation of its target genes as hsa_circ_0007615's mode of action[62].

Contrary to these, circBNC2 and hsa_circ_0001546 were recently reported to exert tumor-suppressing effects in EOC. circBNC2 expression level was significantly lower in EOC tissues, an overexpression was found to decrease proliferative, migrative, and invasive abilities in EOC cell lines. It was confirmed to exert its tumor-suppressing effects by miR-223-3p sponging[63]. Likewise, hsa_circ_0001546 was reported to be downregulated in EOC primary and metastatic tissues and confirmed to function by acting as a protein chaperone, binding 14-3-3 protein[64].

circRNAs have also been highlighted as potential biomarkers and therapeutic targets, including ciRS-7 and circN4BP2L2. ciRS-7 is differentially expressed in EOC tissues, detected in plasma, and capable of miRNA sponging activity[65]. Increased expression of ciRS-7 was also found to be associated with worse overall survival in patients. A low level of circN4BP2L2, on the other hand, was associated with aggressive tumors with increased metastasis, low relative

survival rate, and capability of distinguishing early-stage EOC from benign and normal ovarian tissues[66]. Other known functions of circRNA that directly characterize cancer cells include regulating cell death pathways, stimulating angiogenesis, and largely deregulating cell energetics and metabolism.

1.2.5: Limitations and Advancement in circRNA Research

Although circRNAs are more stable than their linear counterparts, studying them presents more limitations due to their cyclic structure and reduced endogenous abundance, which hinders a comprehensive understanding of their molecular pathways. To begin, RNA isolation steps must be optimized to include enrichment for circRNA (especially for larger circRNAs) by degrading linear RNA through RNase R application when necessary[53]. Due to the absence of mature mRNA modifications, including 5' G-Cap and Poly A tail, cDNA synthesis to detect circRNA through quantitative real-time PCR (qRT-PCR) or next-generation sequencing (NGS) must selectively utilize random hexamers to amplify circRNA. Also, circRNA detection through qRT-PCR or bioinformatic analysis is approached using a technique different from linear mRNA. Primers are designed to bind to BSJ, which is unique to circular isoforms of a target gene, to quantify circRNA expression during qRT-PCR. As such, careful consideration during the design of the primer is required to ensure that only circular and not linear RNA of the target genes are detected[53]. Likewise, alignment techniques that meticulously account for BSJs and enable de novo assembly of circular RNA must be employed for circRNA NGS analysis[53]. Another concern is the overexpression and knockdown of circRNA, as traditional methods are not very effective. Using minigenes containing flanking intronic sequences has been proven sufficient to facilitate circularization[67] and thus increase the expression level of circRNA only. At the same time, shRNA with a sequence complementary to the BSJ effectively reduces their expression.

1.2.6 Potential Diagnostic/Therapeutic Values

Regardless, the potential of circRNA as a novel diagnostic tool and therapeutic target in numerous diseases, including cancer, remains significant. Large-scale bioinformatic analyses have revealed differential expression of circRNAs in diseased vs. regular patients; coupled with their easy detection in bodily serum and fluids and increased stability, numerous studies continue to research their potential as diagnostics biomarkers. For instance, circPVT1 has been suggested as a prognostic marker of gastric cancer[68] and circN4BP2L2 as a diagnostic and prognostic biomarker in EOC[68]. Furthermore, circRNAs could be used as therapeutic targets in cancer as they can exert tumor-promoting and suppressing effects in these tumors. A detailed review of different circRNAs with potentials as therapeutic targets in EOC strongly suggests that they play a role in chemosensitivity, angiogenesis, and overall tumor progression[24].

1.3: SKA3 Gene

1.3.1: Overview of SKA Family

The spindle and kinetochore-associated (SKA) family includes three genes, *SKA1-3*, that primarily regulate chromosomal separation and aid in cell division. *SKA1* and *SKA2* are essential in various cellular processes, including facilitating microtubule binding, aiding chromosomal segregation, and regulating microtubule dynamics by promoting polymerization and depolymerization[69]. Relative to other tissues, an augmented expression level of *SKA1* is noted in bone marrow, while *SKA2* exhibits heightened expression in the brain[70]. Complementing *SKA1* and *2*, *SKA3* is another part of the outer kinetochore that ensures proper chromosomal segregation and cell division.[75]

1.3.1.A: SKA3

SKA3 is located on Chr 13q12.11 and spans 21153595..21176552 chromosome regions. Via alternative splicing, the SKA family of genes produces multiple transcript variants, and together, they form a complex that strengthens kinetochore-microtubule attachment[71]. *SKA3* has 7 transcripts consisting of 29 exons on the reverse strand. Beyond the canonical functions of the SKA family, numerous studies have reported the role of *SKA3* in promoting tumorigenicity in different cancers, including breast, cervical, lung, liver, and skin cancers, by enhancing proliferation, invasion, and cell growth. Despite extensive investigation in other tumors, the role of *SKA3* genes in OC is still unknown.

1.3.2: circular SKA3

Interestingly, the *SKA3* gene is also capable of producing circular RNA transcripts. According to circBase, nine isoforms of circular RNA are derived from back-splicing events of *SKA3* gene in *Homo sapiens* with genomic length ranging from 119-1016 bp. These isoforms possess a coding sequence derived from back-splicing events involving internal exons and introns. Two isoforms of circSKA3 have been reported to increase tumorigenicity in different tumors, including hsa_circ_0000467 in breast cancer [72,73,81], CRC[74–77] and gastric cancer and hsa_circ_0029696 in medulloblastoma[78,79]. Majorly, their mode of action involves miRNA sponging to indirectly regulate the downstream target genes of miRNAs and increase cell proliferation, invasion, and migration abilities.

Hsa_circ_0000467 is an isoform of circSKA3 comprising 412 base pairs derived from exon 4 with sequences predicted to bind and sponge miRNAs (Figure 1.4). It is the most reported isoform of circSKA3 with implications in tumors and was found to be significantly upregulated

in EOC following circRNA sequencing by our collaborators. The *SKA3* gene from which it is derived is known to facilitate cell division, mitotic cell cycle and spindle fibre attachment to kinetochore, thus implicating their crucial role in cellular division. Different isoforms of circSKA3 have been reported to directly interact with proteins such as SLUG to promote EMT[76], β-catenin to activate the wnt signalling pathway in CRC[75], and integrin β1 to induce invadopodium formation and invasive abilities in breast cancer[72]. Furthermore, its knockdown reduced cell proliferation, invasion, migration, and EMT in CRC cells[74]. They have also been reported to interact with different miRNAs, including miR-1[80], miR-326[78], miR-383-5p[79], miR-520-h[81], miR-1238[82], miR-1303[83] and miR-6796-5p[84]. Other potential functions of circSKA3 include being a transcriptional regulator. These findings highlight the role of circSKA3 as an oncogenic circRNA capable of interacting with proteins directly and regulating gene expression levels indirectly via miRNA sponging.

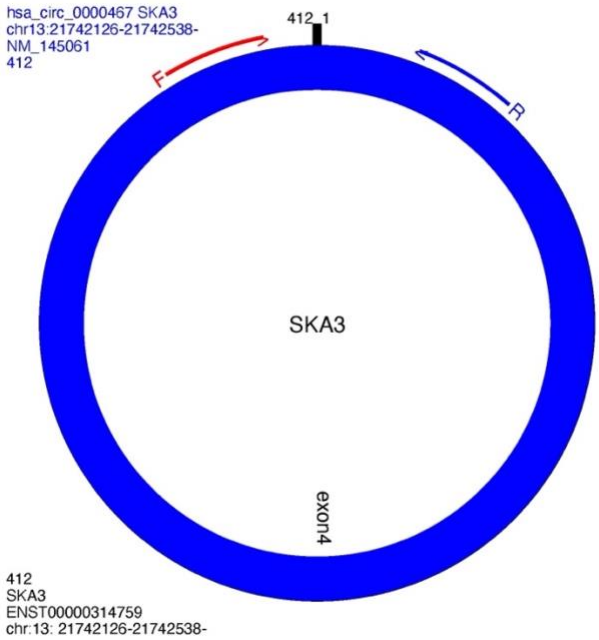

Figure 1.4: Structure of hsa_circ_0000467 isoform produced by back splicing at exon 4.

This isoform is an exonic circRNA derived from exon 4 and is circularized by BSJ, linking the 5' end to the 3' end. They have been reported to promote cancer aggressiveness by protein binding and miRNA sponging activities.

1.4: MicroRNA

1.4.1: Overview of miRNA

miRNAs are small non-coding RNAs (approximately 22 nucleotides) well characterized for their sequence-specific post-transcriptional gene regulation. Their anomalous expression also characterizes numerous diseases, including cancers[85]. They are generated via one of two pathways, including canonical biogenesis, during which pri-mRNA, following transcription, is processed into pre-miRNA by the microprocessor complex. The resulting pre-miRNAs are then exported to the cytoplasm by XPO5/RanGTP complex to be processed into mature miRNA duplex following DICER processing. Other less common miRNA biogenesis pathways are

broadly classified into Drosha or Dicer independent pathways. Pre-miRNAs generated through the Drosha/DGCR8-independent pathway mimic Dicer substrates, directly exported to the cytoplasm via exportin 1 without Drosha cleavage. Conversely, Dicer-independent miRNAs originate from endogenous short hairpin RNA (shRNA) transcripts and necessitate AGO2 for cytoplasmic maturation due to inadequate length for Dicer processing. This facilitates the loading of the entire pre-miRNA into AGO2 for AGO2-dependent slicing, culminating in their maturation[85].

They are capable of gene-silencing via the formation of a miRNA-induced silencing complex (miRISC) consisting of the AGO protein and a guide strand. Depending on the level of complementarity between the guide strand and target gene transcript, the AGO protein silences (high complementarity) or reduces (low complementarity) its translation. Ongoing studies also suggest that miRNAs may play a role in establishing an epigenetic landmark via methylation and chromatin remodelling mechanisms[85]. Conversely, miRNAs have also been reported to increase gene expression levels under specific conditions, including cell cycle arrest and protein starvation[85], and when localized to certain cell regions, including the mitochondria[86]. miRNA sponging by circRNA involves binding to complementary sequences, thus reducing their availability and preventing the regulation of their target genes. Since miRNA dysregulation is a hallmark of cancer, it is suggested that circRNA might regulate cancer development via miRNA sponging.

1.4.2: circRNA-miRNA Interaction

Most circRNAs function via miRNA sponging, including circSKA3. This involves them acting as competing endogenous RNA (ceRNA) to interact with miRNA in a complex regulatory network, leading to significant downstream effects in cancers. Also, this interaction contributes

to hallmarks of cancer, including tumor proliferation, metastasis, angiogenesis, drug resistance, and apoptosis[87]. This highlights the importance of circRNA-miRNA crosstalk as an essential component of cancer regulation. Essentially, the pathway involves a binding interaction facilitated by complementary sequences between circRNA-miRNA, leading to miRNA sponging. This event disrupts miRNA-mRNA interaction as miRNA abundance decreases in the cell, altering cellular expression levels. Ultimately, critical cellular processes are disrupted due to the dysregulation of regular mRNA interaction, which contributes to the tumor microenvironment (TME), suggesting circRNA-associated ceRNA network as a promising avenue for identifying novel cancer biomarkers and therapeutic targets[88].

1.5: Rationale, Objective, and Hypothesis

Despite the increasing understanding of circRNA, their role in EOC remains widely understudied. Understanding the role of circRNAs in EOC is essential as it is the most lethal gynecologic cancer and is often diagnosed at advanced stages due to the lack of definitive symptoms. Given the enhanced stability of circRNAs, they present promising targets for therapeutic intervention and diagnostic biomarkers in EOC.

circSKA3 (hsa_circ_0000467) was observed to be aberrantly expressed in HGSC through a circRNA seq study conducted by our collaborators. Current research elucidates their role in promoting cell proliferation, migration, and invasion capacity in other cancers, including CRC[74,76] glioblastoma[80,89] and breast cancer [72]. It has also been reported to regulate apoptosis in medulloblastoma [79,90]. Preliminary work in our lab suggests that circSKA3 is overexpressed in HGSC compared to LMP tumors. Likewise, we observed a positive regulation of tumor-invasive proliferative abilities by circSKA3 in EOC cell lines, OVCAR3, and CAOV3. Our results further

suggest that circSKA3 might exert tumor-promoting effects by decreasing miR-383-5p levels, as we also observed increased miR-383-5p levels in LMP compared to HGSC. Furthermore, mRNA levels of validated miR-383-5p target genes, including *LDHA* and *SFN*, decreased on knocking down circSKA3 in these cells[91].

Based on the promising result in our lab, we hypothesize that circSKA3 promotes HGSC progression via miRNA sponging and protein interactions. Thus, this research aims to further explore the role of circSKA3 in HGSC development. We examined its expression levels in HGSCs and determined the effects of its overexpression/silencing on EOC proliferation, migration, and invasion. Additionally, we proposed that circSKA3 exerts its tumor-promoting effects by binding to proteins and miRNAs, leading to changes in the downstream molecular pathways. Using *in vitro* and bioinformatic studies, we addressed the following research questions: What is the role of circSKA3 in HGSC progression, and what miRNAs and proteins may interact with it?

CHAPTER 2

MATERIALS AND METHODS

2.1: Cell Culturing

HGSC cell line, OVCAR3, was purchased from the American Type Culture Collection (ATCC), cultured, and used in this study. Cells were maintained in Dulbecco's Modified Eagle Medium (DMEM) (Thermo Scientific cat # 11965118) supplemented with 10% fetal bovine serum (FBS) and incubated at 37°C with 95% air and 5% CO_2, following ATCC guidelines. Additionally, they were subcultured as recommended by ATCC and dependent on cell confluency to ensure optimal cell viability.

2.2: Construction of circSKA3 Overexpression and Knockdown Vector

To overexpress circSKA3, a plasmid featuring flanking inverted repeat elements with high complementarity, an upstream splice acceptor, a downstream splice donor site, and a branch point was designed. pcDNA3.1(+) CircRNA Mini Vector gifted from Jeremy Wilusz lab[92] (Addgene plasmid # 60648; http://n2t.net/addgene:60648; RRID: Addgene_60648) was digested using EcorV (NEB Cat #R0195S) and SacII (NEB Cat #R0157S) enzymes. Digestion was optimized as follows to increase precision and concentration of digested to undigested plasmids; 1ug of plasmid DNA was combined with 1ul SacII, 2ul EcorV, 2.5ul of 10X NEBuffer r2.1 (NEB Cat # B6002S) and nuclease-free water (NFW) up to 20ul and incubated at 37°C for 2 hours. The digested vector was visualized on 1.7% agarose gel and isolated via DNA gel extraction using Monarch gel extraction kit (NEB Cat # T1020L).

Primers containing short protective oligonucleotides and EcorV and SacII RE site flanking SKA3 exon sequence were designed as listed in Supplementary Table A1.1. circSKA3 exonic mRNA sequence containing flanking restriction enzyme (RE) site was then synthesized by amplifying a plasmid containing *SKA3* exon 4 sequence via PCR with Q5 high fidelity (HF) polymerase (NEB Cat #M0251S) following the manufacturer's protocol. The sequence was

visualized on 1.7% agarose gel, isolated via DNA gel extraction using Monarch gel extraction kit (NEB Cat # T1020L), and digested as described earlier. Using NEB Ligation calculator (required mass insert (g) = desired insert/vector molar ratio x mass of vector (g) x ratio of insert to vector lengths), digested circSKA3 insert and vector were incubated at a 7:1 ratio at room temperature for 2 hours using T4 DNA ligase (NEB Cat #M0202) according to the manufacturer's protocol. By incubating at 65°C, the ligation was inactivated. Following the manufacturer's protocol, 5ul of the ligate was transformed into 50ul of NEB Stable Competent cells (NEB Catalog #C3040H) and incubated at 37°C overnight using ampicillin selection plates. Negative controls of ligated vector or circSKA3 insert only were also plated and cultured similarly.

Seven colonies on the vector+circSKA3 ligated plates were selected, and the presence of the circSKA3 insert sequence was tested via colony PCR using primers flanking *SKA3* exon 4 sequence. Briefly, colonies were picked with a clean pipette tip and inserted into tubes containing 5ul NFW at 60°C for five minutes. The solution was then combined with primers for the flanking sites and *SKA3* mRNA; PCR was carried out using Q5 HF polymerase (NEB Cat #M0251S) following the manufacturer's protocol, and samples were visualized on 1.7% agarose gel. 5 colonies positive for the circSKA3 sequence as seen on the gel were randomly selected and sent to the centre for applied genomics (TCAG) for DNA sequencing following their recommended protocol. Based on the sequencing results, 1 of the clones was expanded and frozen in glycerol, and plasmid DNA was extracted for use in this study.

shRNA construct containing sequences complementary to circSKA3 BSJ was also designed for stable knockdown. The construct was designed using a validated siRNA sequence targeting circSKA3 BSJ efficiently and capable of reducing its expression transiently. The siRNA sequence was cloned into pGPU6/GFP/Neo plasmid and ordered from Gene Pharma Co.

Similarly, negative control containing scrambled sequence with no known/predicted complementary site was designed and ordered from Gene Pharma Co. Sequences are included in Supplementary Table A1.2

2.3: Transient Transfection

OVCAR3 cells were seeded evenly at a density of 1.5×10^5 in 6 well plates (SARSTEDT, cat #83.3920300), each well containing 2ml of culture media. On attaching to the wells, cells were incubated overnight and transfected the following day. Following Lipofectamine™ 3000 (Fisher Scientific cat #L3000015) standard protocol, transfection mixes for appropriate plasmids and their controls (circSKA3 and empty vector or shcircSKA3 and shNC) were prepared. In the first tube, 2.5µg of plasmid, 5µl of P3000, and 125µl of Opti-MEM (Thermo Scientific cat #31985088) were combined for each well. 7.5µl of Lipofectamine™ 3000 was diluted in the second tube in 125µl Opti-MEM. Both tubes were combined by adding tube 1 into tube 2, mixing, and incubating at room temperature for 15 minutes. During the incubation, media was changed to 750µl Opti-MEM for each well, and 250µl of the transfection mix was added after incubation. Six hours post-transfection, the transfection mixture was replaced with their culture medium.

2.4: Stable Transfection

Cells were seeded and transiently transfected to generate OVCAR3 knockdown, and overexpression stable cell lines as described above. Forty-eight hours post-transfection, cells were washed with 1X PBS, and media containing 500µg/ml of G418 (Thermo Scientific cat #10131027) was added to select transfected cells. Selection continued for two weeks with media change every 3-4 days following visual inspections to assess cell growth and confluency. Selected cells were seeded at 1 cell/well into 96 well plates and cultured with culture media +

250µg/ml for maintenance. At about 90% confluency, monoclonal cells were detached using TrypLE™ express enzyme (Gibco cat # 12604013) and transferred to a 100mm^2 dish (SARSTEDT cat #83.3902.300) to expand. Once confluent, cells were passaged, and RNA was isolated from the remaining cells to measure the expression level of circSKA3 via qRT-PCR. Following the results, cells with the lowest and highest expression levels were continuously subcultured with 250µg/ml of G418 in culture media and used for other experiments.

2.5: RNA Extraction, Reverse Transcription, and Real-Time PCR

Total RNA was extracted from cells and tissues using Monarch Total RNA extraction kit (NEB cat #T2010S) based on the suggested manufacturer's protocol. The RNA samples were quantified and assessed for quality based on their absorbance ratios at 260/230 nm and 260/280 nm. 1ug of pure total RNA (A260/280 & A260/230 ≈ 2) was reverse transcribed into 20ul cDNA using iScript cDNA Synthesis Kit (Bio-Rad cat # 1708891), containing random hexamer and poly A primers, following the manufacturer's protocol. Afterwards, qRT-PCR was carried out using GB-Amp™ Sybr green qPCR mix (GeneBio Product #P2092) or PowerTrack™ SYBR Green Master Mix (Thermo Scientific cat #A46111) and the appropriate forward and reverse primers (10µM) in a 20ul reaction. Thermocycling conditions were set as recommended by manufacturers, with an annealing temperature of 60°C for 35 cycles and melting analysis included using Applied Biosystems™ QuantStudio™ 6 Flex Real-Time PCR System (Catalog # 4485697). The relative expression levels of target genes were analyzed using the $2^{-\Delta\Delta Ct}$ method. *GAPDH* and *18s* were used as endogenous internal controls for cell and tissue samples, respectively. Primer sequences are provided in the appendix (Supplementary Table A1.1).

2.6: Functional Assays

2.6.1: Proliferation Assay

100µl of OVCAR3 stable cells were seeded at a low density of 3×10^4cells/ml into 96 well plates (Greiner Bio-one cat #655180) with a sample size of 30 wells per experimental condition. Following attachments of the cell, proliferation was assessed by taking periodic scans of the cells (every 2 hours) using IncuCyte S3 imaging system. To ensure the cells were healthy, media (containing 250µg/ml G418) was changed every two to three days until they reached 100% confluency. 1X PBS was also added to surrounding wells to maintain humidity. With confluency as the parameter, proliferation curves were generated using Incucyte automated proliferation analysis.

2.6.2: Wound Healing Assay

To analyze cell migration, 100µl of OVCAR3 stable cells were seeded at a very high density of 2.5×10^5cells/ml into Incucyte image lock 96 well plates (SARTORIUS cat #BA-04855) with a sample size of 30 wells per experimental condition. Cells were then incubated overnight to reach 90-100% confluency. The next day, cells were scratched in the middle to make a wound using the Incucyte WoundMaker™ tool. After making the wound, floating cell debris was washed off with DMEM only, and the media was changed to DMEM + 1% FBS only. 1X PBS was added to surrounding wells to maintain humidity. Afterwards, images were taken every 2 hours for 48 hours using Incucyte, and migration curves, with wound confluency as the parameter, were generated.

2.6.3: Clonogenic Assay

Survival and proliferative abilities of individual colonies were evaluated using clonogenic assays. 2 ml of 500 OVCAR3 cells/ml solution in culture media + 250µg/ml G418 was

distributed evenly to each well in six-well plates (SARSTEDT, cat #83.3920300). Cells were then incubated for 7 days with media changed every 3 days. On the 7th day, the clonogenicity of cells was analyzed by fixing and staining using Harleco Hemacolor Staining Kit (Millipore Sigma cat #65044A-85), capturing images of the plates, and manually counting visible colonies.

2.7: Human Epithelial Ovarian Cancer Samples

Epithelial ovarian cancer tissues (n=101) were kindly supplied by Dr. Barbara Vanderhyden from the University of Ottawa and Ottawa Hospital Research Institute's Center for Cancer Therapeutics, Ottawa, ON, with approved patient consent. The samples encompassed a variety of histopathological types, including LMP serous tumors (n=36), HGSC (n=40) and serous cystadenofibroma (CAF) (n=25). Detailed patient information was recorded, including description, diagnosis age, tumor grade, stage, nature, notable markers, metastasis, chemotherapy regimen, resistance profiles, and progression-free intervals.

Total RNA was extracted from all samples using Monarch Total RNA extraction kit (NEB cat #T2010S) following the manufacturer's protocol for tissue samples. Briefly, samples were homogenized while immersed in dry ice for 2-3 minutes, with 15-second breaks after every minute. DNA and protein contaminants were removed using the spin columns and included reagents, and RNA was cleaned and eluted using DEPC water and stored at -80ºC. cDNA was synthesized for all samples with concentration ≥ 67ng/µl and A230/280 ≥ 1.8. This involved reverse transcription of 2µg of total RNA using the iScript cDNA synthesis kit (Bio-Rad cat # 1708891), with resulting cDNA stored at -20ºC.

2.8 circSKA3 Binding Protein Pulldown

To identify novel circSKA3-protein interaction, a pulldown assay using a circSKA3 BSJ probe was carried out as outlined by Li et al.[93] with notable optimizations listed below. To begin,

a back splicing probe containing four repeats of circSKA3 BSJ sequence and a control probe containing four repeats of random sequences were designed and cloned into pUC57 plasmid by Gene Pharma Co (Supplementary Table A1.2). Bacterial transformation, inoculation, and plasmid extraction were performed to amplify the probe plasmids using plasmid Maxi kit (Qiagen cat #12162). Biotin-labeled nucleotides were then incorporated into the probe using Q5 polymerase with 2µl biotin-labeled dCTP (Jena Bioscience cat # NU-809-BIO16-L), 0.4µL dNTP (2A:2T: 2G:1C), 4:1 (Reverse: Forward) primer ratio in 20ul reaction using standard thermocycling conditions and appropriate controls (no plasmid or no biotin dCTP). After PCR, probes were visualized on 1.7% agarose gel and cleaned using Monarch PCR cleanup kit (NEB cat #T2010S).

Cell lysates for pulldown were prepared by culturing OVCAR3 cells to 90% confluency using twenty 100mm diameter dishes and transfecting them with 2.5µg plasmid (circSKA3 or empty vector) as described earlier. 48 hours post-transfection, RNA was extracted from 3 random plates, and circSKA3 expression level was confirmed via qRT-PCR. Using lysate buffer with proteinase inhibitors added (1µM NaF, Na_3VO_4, and PMSF), cell lysate was extracted via sonication, and cell debris was isolated. The biotin-labelled probe was pretreated by rapidly heating at 95ºC and transferring to ice-cold water to separate into single strands. A single-stranded probe was then incubated with cell lysates overnight at 4 degrees with gentle shaking. circSKA3 interacting proteins were pulled down from cell lysate + probe mixture by incubating with Streptavidin magnetic beads (NEB cat #S1420S) at room temperature for 1 hour following pre-treatment with washing solutions (Buffer A and B). After thoroughly washing the pulled-down solution, streptavidin beads were isolated and prepared for mass spectrometry (MS).

2.9: Mass Spectrometry

The eluted streptavidin beads were digested, and ZipTip™ was processed to prep the samples for mass spectrometry. Streptavidin beads were digested using S-Trap™ midi column kit, then purified and concentrated using ZipTip™ pipette tips and processed by the MS Facility at YSci core. All samples were carefully prepared and processed in triplicates.

2.10: Bioinformatic Analysis

2.10.1: circSKA3-miRNA-mRNA prediction

A possible circSKA3-miRNA-mRNA interaction axis was predicted via bioinformatic analysis. The protocol followed for this analysis involved fetching two bulk RNAseq data from Sequence read archives (SRA) (SRP351968[94] and SRP199722[95]) for a total of 15 samples, including HGSC ovarian tissues (n=9) and normal ovaries (n=6). These reads were selected as their RNA processing and sequencing approach allowed retention of total RNA, including those without polyA modifications, allowing for broad detection of numerous RNA transcripts. Using command line prompts following the CIRIquant pipeline[96], the reads were aligned and trimmed using BWA-MEM and HISAT2 indexes, circRNAs were detected using BSJ and front splicing junctions (FSJ) reads, linear RNA was detected using conventional gene counting approach, and a gene count table for circular and linear RNA was generated. Using DESeq2[97] package, differential expression analysis was performed in R. Differentially expressed genes (DEG) from both samples were identified using $p < 0.05$ and log fold change (LFC) > 0.5 and selected as possible mRNA targets of circSKA3 binding miRNAs. Predicted circSKA3 binding miRNAs were then fetched from the CircInteractome database, and target genes for all 15 miRNAs with context+score percentile of ≥ 90 were fetched, combined, and compared to the list of differentially upregulated genes compiled earlier. Upon comparison and clustering, predicted

miRNA and their mRNA targets were exported to Cytoscape, and a network diagram was created for analysis. The methodology is summarized below (Figure 2.1)

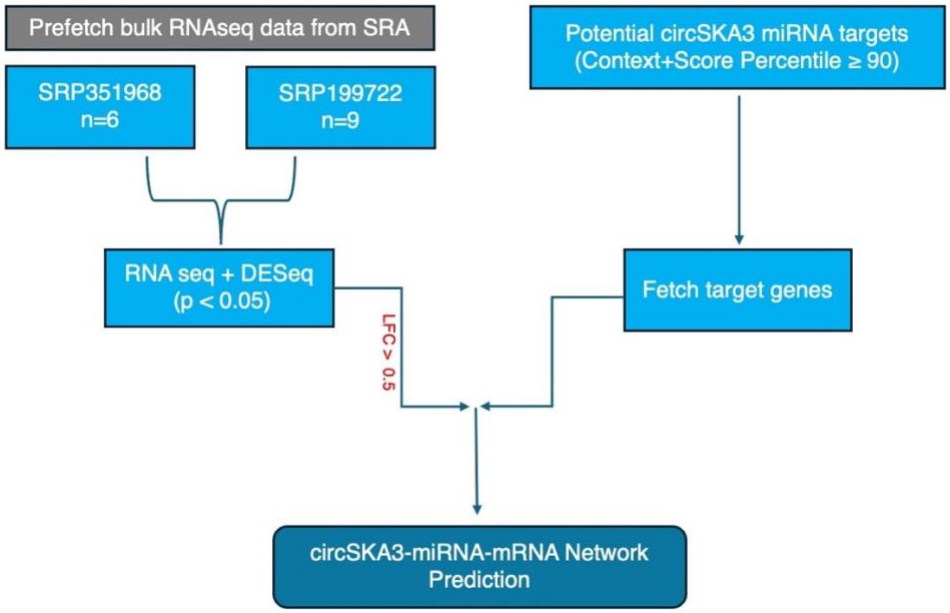

Figure 2.1: Methodology for predicting a circSKA3-miRNA-mRNA interaction axis.

A schematic representation of the methodology used to predict a potential circSKA3-miRNA-mRNA interaction axis via bioinformatic analysis. The resulting miRNA-mRNA interaction network was visualized using Cytoscape for further analysis.

2.10.2: Quantitative Proteomic Analysis

The abundance value of protein hits from MS data was analyzed using MSstats[98] package in R. Briefly, peptide list, spectral count and intensity report were generated by the MS facility at YSci core. Using unique peptides with >1 charge and features and removing runs with >50% counts missing, protein abundance was calculated. Heat map was generated in R to visualize proteins statistically significant or consistently present across groups of samples. Additionally, a network diagram was created using Cytoscape with ClueGO and CluePedia plugins, with a minimum GoTree interval and a cluster of 2 with a maximum level of 18 proteins, to identify functional protein networks and associated pathways.

2.10.3: Gene Ontology (GO) Analysis

All GO analysis for roles of proteins or mRNA in biological processes and molecular function was performed using Functional Enrichment (FunRich) analysis tool v 3.1.3. For protein analysis, protein names were converted to gene names using the Uniprot database, and enrichment and analysis were performed by FunRich. Similarly, a list of mRNAs was imported, and FunRich performed enrichment and analysis.

2.11: Statistical Analysis

Statistical analysis and graph generation were conducted using GraphPad Prism 10.0. Significance was determined at $p<0.05$ level, and the results are presented as mean ±SEM of replicate wells within a single experiment. Each experiment was independently repeated two or more times to ensure consistency in the results. Student's t-test was employed to compare two groups, while One-way ANOVA, followed by multiple comparison tests, was utilized to analyze various groups.

To analyze the mRNA levels measured by RT-qPCR in clinical samples, mRNA levels measured via RT-qPCR were analyzed using the $2^{-\Delta\Delta Ct}$ method following pre-processing of ct values. First, raw ct values with threshold set automatically by Applied Biosystems™ QuantStudio™ 6 Flex Real-Time PCR System (Catalog # 4485697) were imported and sorted by tumor types. Samples with inconsistent ct values or ct values >31 were excluded to ensure reliability. After filtering, Δct was calculated using 18s rRNA levels as endogenous control, and ΔΔct was calculated using CAF tissues as calibrator group. Fold change (FC) was determined using $2^{-\Delta\Delta Ct,}$ and data points with regression values >2 standard deviations from the median FC were removed using the robust regression and outlier removal (ROUT) method to maintain

tumor heterogeneity and increase analysis accuracy. Following outlier removal, FC distribution was determined to be lognormal via normality test. As such, significance was calculated using ordinary one-way ANOVA with Tukey's multiple comparisons test between all groups on log-transformed values of the FCs. All analysis, transformation, and graphing were done using GraphPad Prism 10.

Command line packages (BWA-MEM, HISAT2, DESeq and CIRIquant) were fetched and run on Cedar clusters provided by the Digital Research Alliance of Canada (alliancecan.ca). For all statistical analysis; ns; not significant, *, $p < 0.05$; **, $p < 0.01$; ***, $p < 0.001$; ****, $p < 0.0001$ represent statistical difference.

CHAPTER 3

RESULTS

3. 1: Validation of circRNA-seq Results

To validate the circRNA-sequencing result from our collaborators indicating overexpression of circSKA3 in HGSC, I measured the expression level of circSKA3 and its linear isoform in EOC tissue samples obtained from the Ottawa Ovarian Cancer Tissue Bank (Supplementary Table A1.3) via qRT-PCR. Results confirmed a significant increase in circSKA3 levels by 10 folds in the most aggressive subtype of EOC (HGSC) compared to benign CAF and about 5 folds compared to tumors of LMP (Figure 3.1A). However, the expression level of linear SKA3 mRNA was not significantly different among the tumor groups (Figure 3.1B)

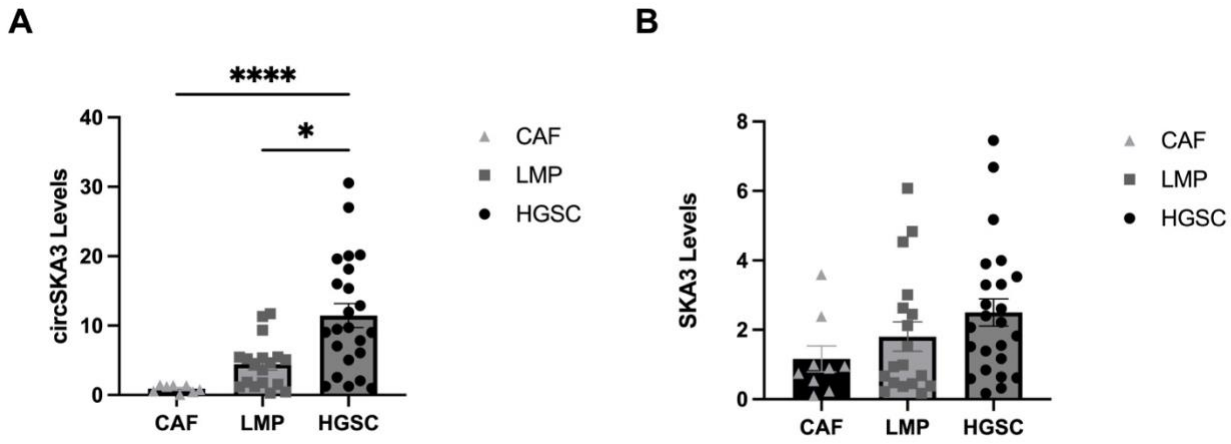

Figure 3.1: Endogenous expression level of circSKA3 and SKA3 in tumor samples.

A) mRNA expression level of circSKA3 is significantly increased in HGSC (n=24) compared to CAF (n=9) and LMP tumors (n=18). B) mRNA expression level of *SKA3* does not exhibit significant differences between LMP, CAF and HGSC samples. Data obtained from qRT-PCR analysis of tumor samples using the ΔΔct method and represented as individual values in dots with mean as bar ± SEM. *, $p<0.05$; ****, $p<0.0001$.

3.2: circSKA3 Overexpression Plasmid Development

Following confirmation of circSKA3 overexpression in HGSC and coupled with previous work in our lab validating its expression levels in ovarian tumor samples and cell lines, subsequent phase involved establishing cell lines with stable circSKA3 knockdown or expression. circSKA3 overexpression plasmid was developed by inserting *SKA3* exon 4 mRNA (Figure 3.2C) into the pcDNA 3.1 mini vector (Figure 3.2B) following digestion of the plasmid (Figure 3.2D) as illustrated in Figure 3.2A. *SKA3* exon with SacII and EcorV flanking site was generated using cDNA samples from OVCAR3 cell lines or a plasmid containing the exon 4 insert, as seen in Figure 3.2C. This was inserted into the digested pcDNA 3.1 circRNA mini vector plasmid (Figure 3.2D).

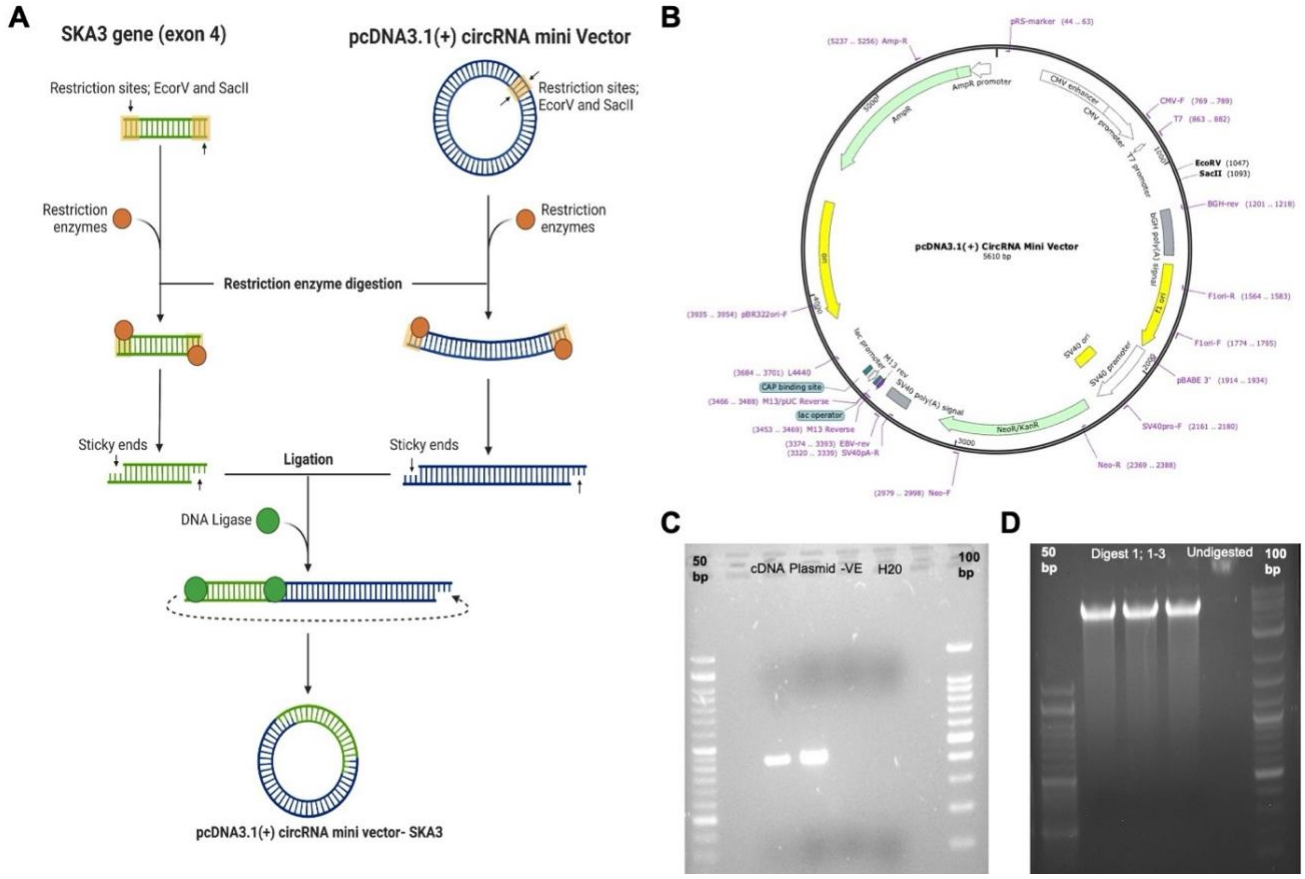

Figure 3.2: Construction of circSKA3 overexpression plasmid.

A) Schematic representation of the construction process, illustrating the insertion of *SKA3* exon 4 mRNA into the pcDNA 3.1 mini vector. B) pcDNA 3.1 circRNA mini vector construct used as the backbone for circSKA3 overexpression plasmid development. C) Generation of *SKA3* exon 4 mRNA insert from cDNA samples or plasmid. D) Digestion of the pcDNA 3.1 circRNA mini vector plasmid to facilitate the insertion process.

The sticky ends of both digests were ligated using T4 DNA ligase with an insert-to-vector ratio of 7:1 and transformed into NEB-stable competent cells. After transformation, competent cells were plated onto bacteria agar plates, and random colonies were chosen for colony PCR to verify successful and proper ligation of the insert to vector. Seven colonies were selected from

the vector+insert ligate plates, all of which showed up positive for the *SKA3* sequence, a colony from vector-only ligate was also tested and showed up absent for the *SKA3* sequence (Figure 3.3A). Plasmid was extracted from some of the colonies positive for *SKA3* and sent for sequencing which confirmed 100% match of the sequence and orientation (Figure 3.3B &C).

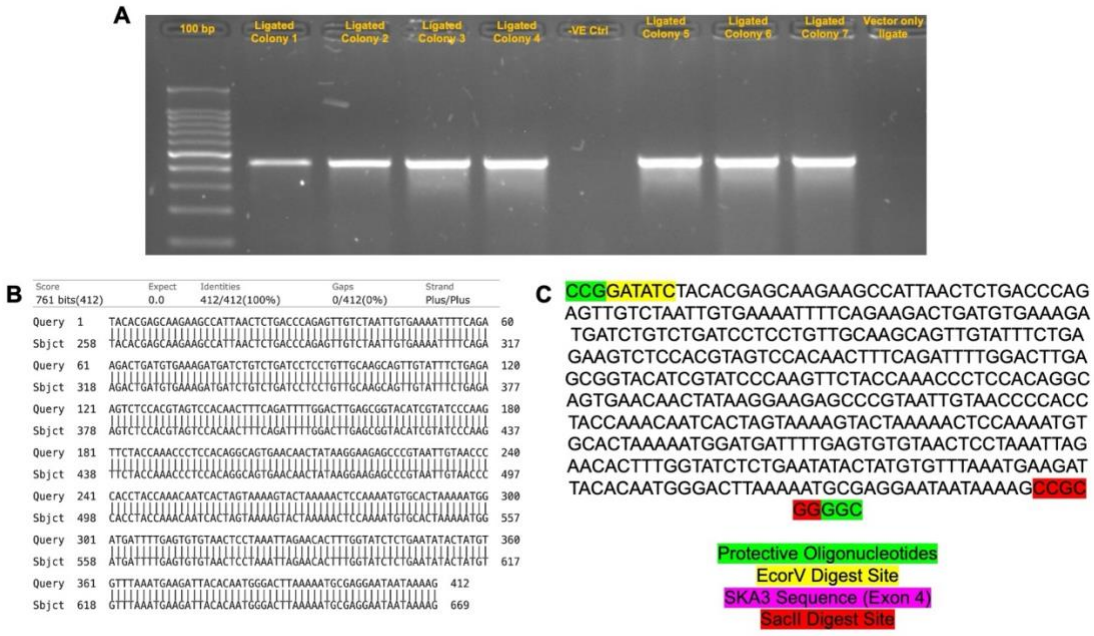

Figure 3.3: Validation of circSKA3 overexpression plasmid construction.

A) Colony PCR results confirming successful ligation of *SKA3* insert to vector in selected colonies, with absence of *SKA3* sequence in vector-only control colony. B) BLAST analysis of the sequencing results showing 100% match with the expected *SKA3* sequence. C) Sequence detail for *SKA3* mRNA + flanking RE sites and protective oligonucleotide.

3.3: Overexpression and Knockdown of circSKA3 in HGSC Cell Line

OVCAR3 cells were transiently transfected with either circSKA3 overexpressing plasmid and vector-only control or shCircSKA3 construct and negative control to develop stable cell lines following continuous selection. Transfection was carried out as described in the materials

and methods section, followed by RNA extraction and qRT-PCR to confirm the levels of circSKA3 at 48 hours post-transfection. Using 2.5ug of the shCircSKA3 construct, circSKA3 expression was reduced by 50% compared to the negative control (Figure 3.4A). Likewise, circSKA3 was overexpressed by over 150 folds in cells transfected with 2.5ug of the overexpression construct compared to empty vector (Figure 3.4B).

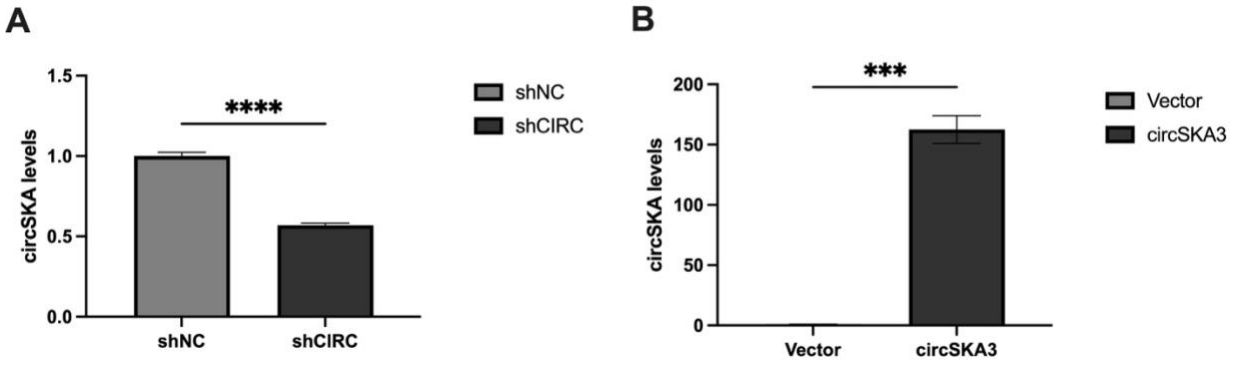

Figure 3.4: Validation of circSKA3 overexpression and knockdown in OVCAR3 Cells post transient transfection.

A) qRT-PCR analysis shows a 50% reduction in circSKA3 expression following transfection with shCircSKA3 construct compared to negative control. B) Overexpression of circSKA3 by over 150-fold was observed in cells transfected with circSKA3 overexpression plasmid compared to empty vector control. Data was obtained 48 hours post-transfection and expressed as mean ± SEM following analysis using the ΔΔct method (n=3). ***, $p < 0.001$; ****, $p < 0.0001$

Transiently transfected cells were continuously cultured and selected to establish stable cell lines using G418. Monoclonal stable cell lines were generated after two weeks of selection, isolation, and expansion. Subsequently, RNA was extracted from these cell lines, and circSKA3 level was measured via qRT-PCR, confirming reduced expression by 60% in knockdown cells (Figure 3.5A). In contrast, overexpression cell lines exhibited approximately an 8-fold increase in circSKA3 expression levels (Figure 3.5B).

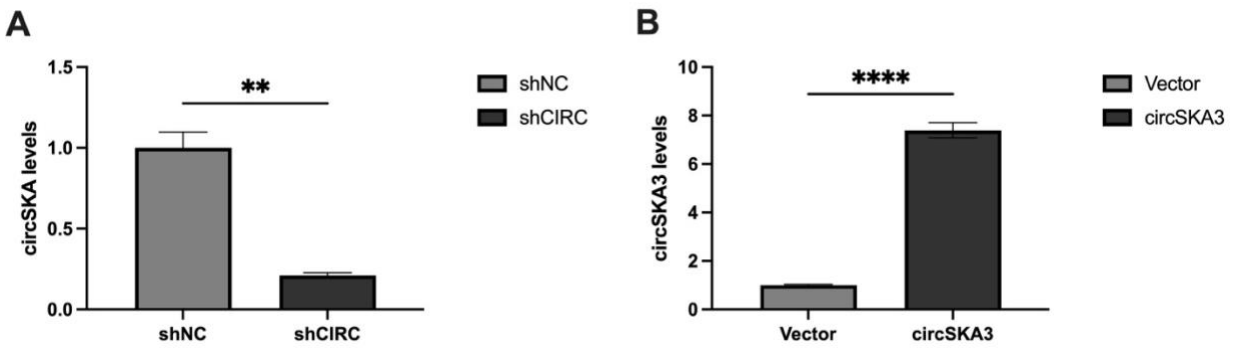

Figure 3.5: Validation of circSKA3 overexpression and knockdown in OVCAR3 stable cell lines.

A) qRT-PCR analysis shows ~70% reduction in circSKA3 expression following stable transfection with shCircSKA3 construct compared to negative control. B) Overexpression of circSKA3 by approximately 8 folds observed in cells transfected with circSKA3 overexpression plasmid compared to empty vector control. Data was obtained following the selection and expansion of stable cell lines and expressed as mean ± SEM following analysis using the ΔΔct method (n=3). **, $p < 0.01$; ****, $p < 0.0001$.

3.4: circSKA3 Effect on Proliferation, Migration and Clonogenicity

Upon developing stable cell lines expressing circSKA3 at increased and decreased levels, functional assays were carried out to investigate how this might alter hallmarks of cancer. Proliferation assay was carried out using both circSKA3 overexpressed and knockdown cell lines and their appropriate controls. Knocking down circSKA3 led to a significant decrease in the proliferative abilities of OVCAR3 cells compared to cells transfected with the negative control. Interestingly, significant differences in proliferative abilities were observed from about 10 hours till the end of the assay (Figure 3.6A). However, overexpression of circSKA3 by ~8 folds in the overexpression stable cell line led to no significant difference in their proliferative abilities compared to control cells (Figure 3.6B).

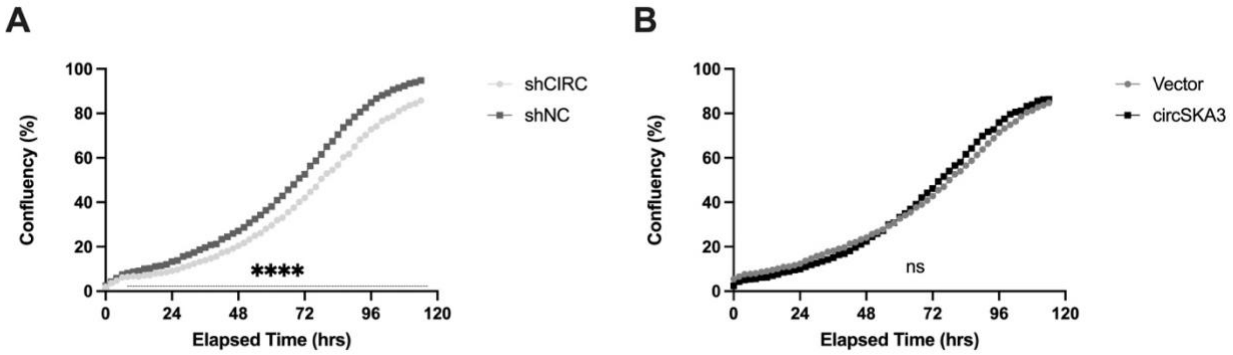

Figure 3.6: Impact of circSKA3 levels on proliferative abilities of OVCAR3 cells.

A) Knockdown of circSKA3 significantly decreases proliferative abilities compared to negative control cells, with notable differences observed from approximately 10 hours onward. B) Overexpression of circSKA3 by ~8-fold does not significantly alter proliferative abilities compared to control cells. Data obtained from proliferation assays using stable cell lines expressing varied levels of circSKA3, monitored using IncuCyte imaging system and expressed as mean ± SEM (n=30). ns, not significant; ****, $p < 0.0001$.

The effect of circSKA3 expression levels on the migrative abilities of OVCAR3 cells was also evaluated by carrying out a wound-healing assay using stable cell lines. Results indicate a significant decrease in migrative abilities in cells with reduced expression of circSKA3 after the first two hours till the end of the assay (Figure 3.7A). Likewise, a significant increase was observed in the migrative abilities of cells with increased expression of circSKA3 from the first two hours, with wound confluency level approaching a climax of ~90% for both cells after 40 hours (Figure 3.7B).

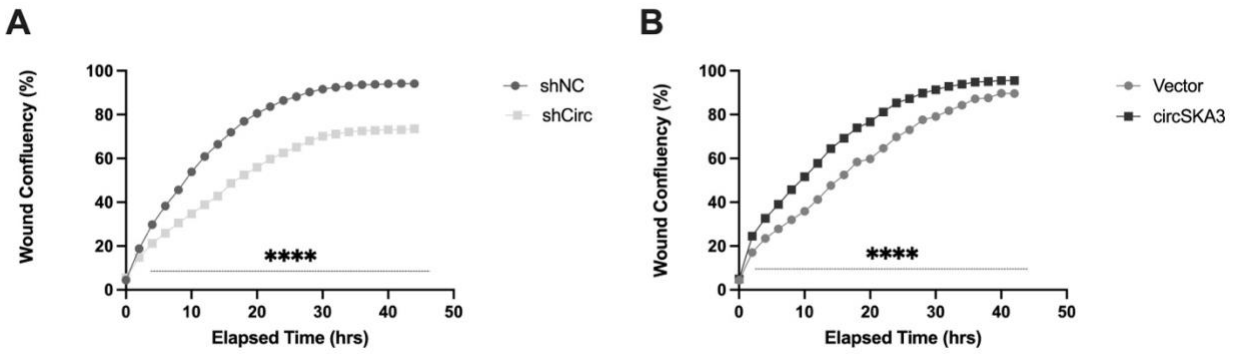

Figure 3.7: Impact of circSKA3 levels on migrative abilities of OVCAR3 Cells

A) Knockdown of circSKA3 significantly decreases migrative abilities compared to negative control cells, with notable differences observed from 2 hours post-wound scratching. B) Overexpression of circSKA3 significantly increases migrative abilities compared to control cells from 2 hours post-wound scratching. Data obtained from migration assays using stable cell lines expressing varied levels of circSKA3, wound confluency was monitored using IncuCyte imaging system and expressed as mean ± SEM (n=30). ****, $p < 0.0001$.

To assess the abilities of individual OVCAR3 cells to proliferate and form their colonies over an extended period, stable cells with varying circSKA3 expression levels were seeded at low density and allowed to form colonies. Upon analyzing the number of colonies produced, the number of colonies produced correlated with circSKA3 levels as a decrease in number of colonies was observed in knockdown cells compared to control (Figure 3.8 A&C) while an increase was observed in overexpression cell lines (Figure 3.8 B&D)

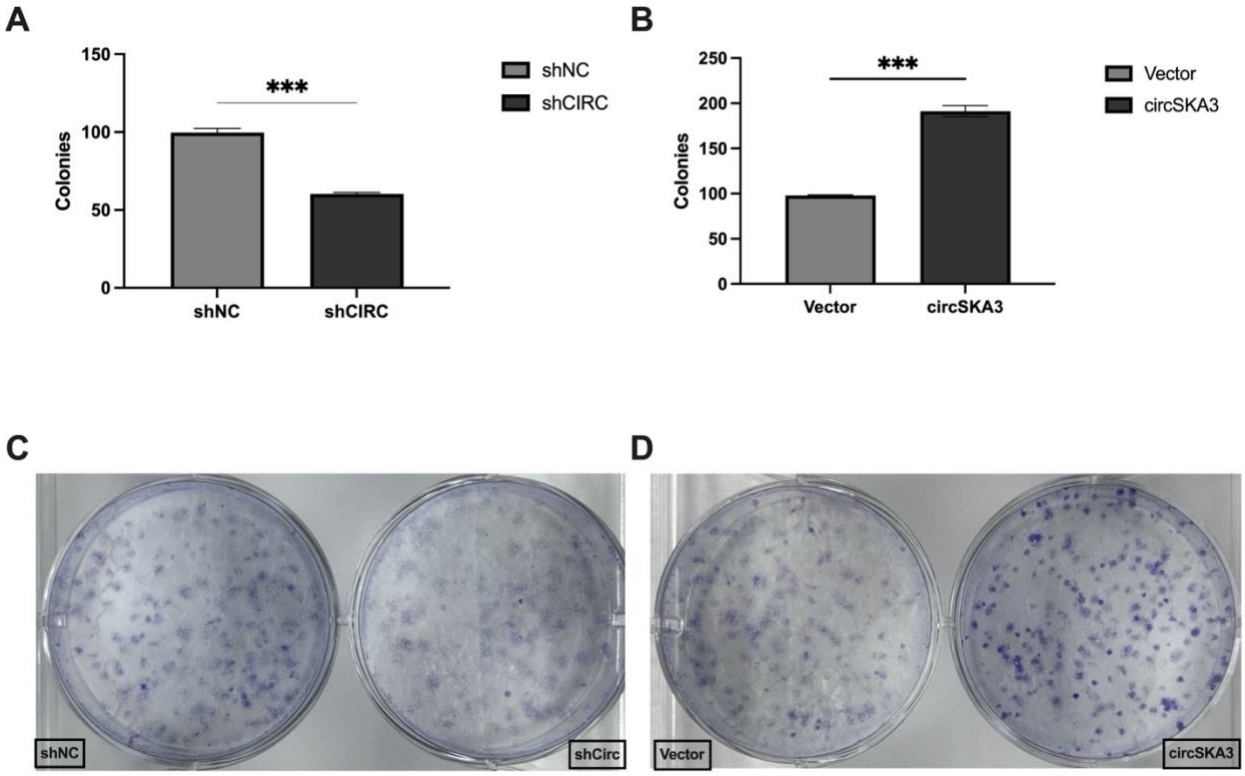

Figure 3.8: Impact of circSKA3 expression levels on clonogenicity of OVCAR3 Cells.

A) Colony formation abilities significantly decreased in stable cell lines with decreased expression of circSKA3 compared to control. B) Significant increase in colony formation abilities observed in cell line overexpressing circSKA3. C) Representative images of colonies from knockdown cell line and control. D) Representative image of colonies from overexpression cell line and control. Data obtained from counting colonies formed 7 days post-transfection and expressed as mean ± SEM (n=3). $p < 0.001$; ***

3.5: EMT Markers Expression Level in HGSC

EMT is a critical process in tumor progression, which aids the development of invasive and metastatic properties in cancer cells. It is often correlated with tumor aggressiveness and might predict patient outcomes[99]. As such, the expression level of epithelial markers, *E-Cadherin* (*ECAD*), and mesenchymal markers, *N-Cadherin* (*NCAD*), *SNAIL* and *SLUG*, were measured from tumor samples via qRT-PCR. Results confirmed a significant decrease in *ECAD* mean expression level in HGSC compared to tumors of LMP (Figure 3.9A). However, *ECAD* levels were also higher in CAF. No significant difference was observed in *NCAD* (Figure 3.9B) and SNAIL (Figure 3.9C) mRNA levels among CAF, LMP, and HGSC samples. Surprisingly, SLUG mRNA levels were significantly downregulated in HGSC and LMP when compared with CAF and HGSC as compared to LMP (Figure 3.9D).

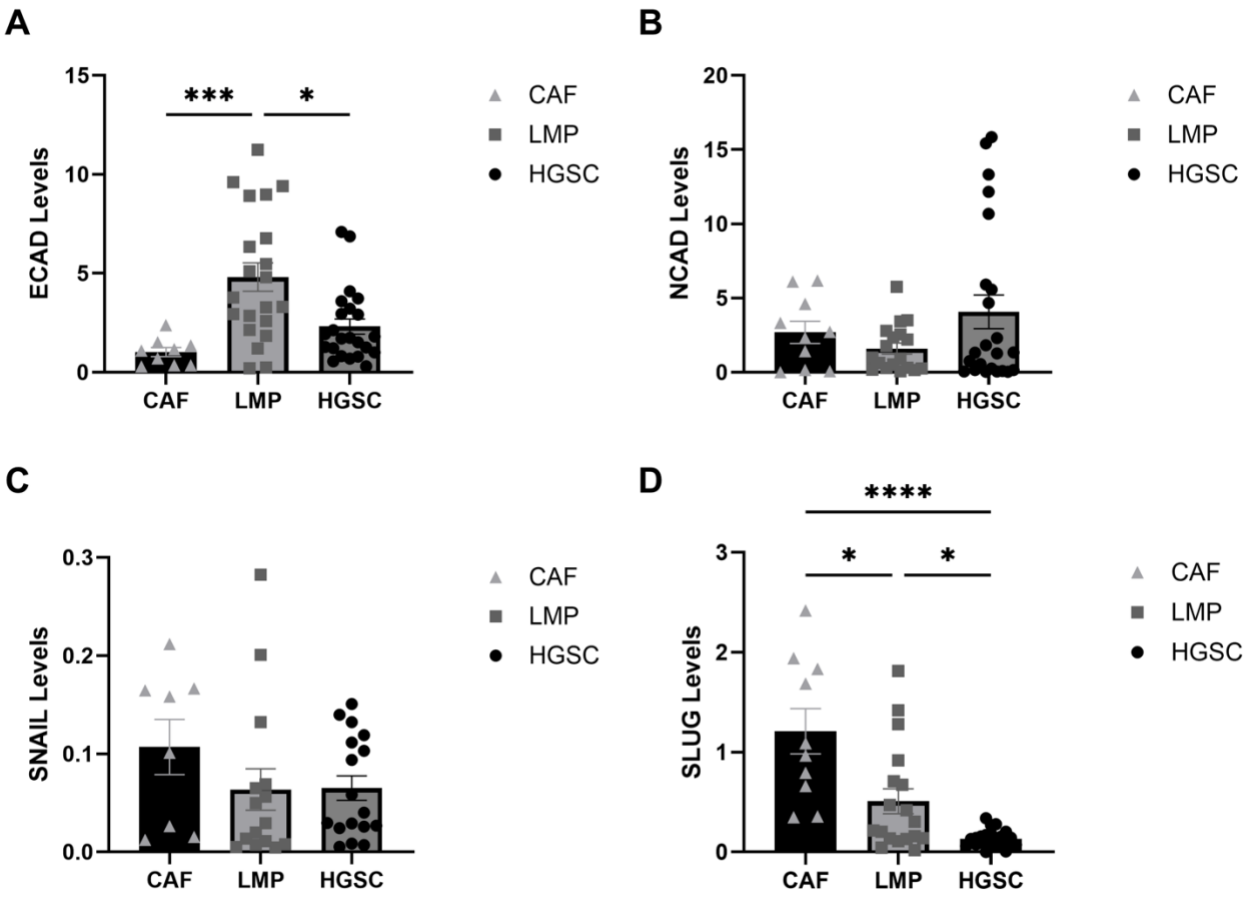

Figure 3.9: Expression levels of EMT markers in ovarian tumor samples.

A) Significant decrease in *ECAD* expression observed in HGSC (n=24) and CAF (10) compared to LMP tumors (n=22). B) *NCAD* levels show no significant difference, with higher mean expression in HGSC (n=24) compared to CAF (n=10) and LMP (n=22). C) No significant difference in *SNAIL* expression, with the highest mean levels in CAF (n=8), followed by LMP (n =15) and HGSC (n=17). D) Significant upregulation of *SLUG* expression in CAF (n=10) compared to HGSC and LMP (n=18) and in LMP compared to HGSC (n=24). Data obtained from qRT-PCR analysis of tumor samples using the ΔΔct method and represented as individual values in dots with mean as bar ± SEM. *, $p < 0.05$; ***, $p < 0.001$; ****, $p < 0.0001$.

Alongside, the expression levels of MUC16, which encodes CA-125, a marker of tumor progression, were measured in the tissue samples to provide information on tumor heterogeneity and behaviour. Results show a significant increase in the mean expression level of MUC16 in

LMP and HGSC compared to CAF as seen in Figure 3.10A. However, MUC16 mRNA levels were not significantly different between LMP and HGSC tumors.

LDHA expression levels were also measured as previous work in our lab implicates their contribution to the circSKA3 mode of action in OC[91]. Furthermore, LDHA expression is associated with increased tumor metabolism related to the Warburg effect. qRT-PCR analysis shows a significant increase in LDHA levels in LMP and HGSC compared to CAF tissues, but similar levels were observed between LMP and HGSC tumors (Figure 3.10B).

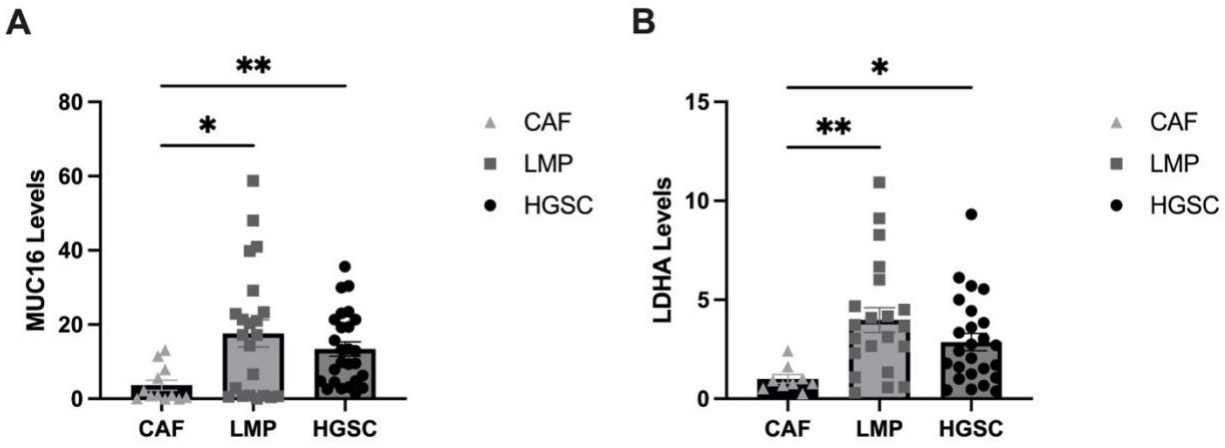

Figure 3.10: Expression levels of MUC16 and LDHA in ovarian tumor samples.

A) Significant increase in the mean expression level of MUC16 observed in LMP (n=22) and HGSC (n=27) tumors compared to CAF (n=12) tissues. B) qRT-PCR analysis reveals a significant increase in LDHA levels in LMP (n=21) and HGSC (n-26) tumors compared to CAF (n=9) tissues. Data obtained from qRT-PCR analysis of tumor samples using the ΔΔct method and represented as individual values in dots with mean as bar ± SEM. *, $p < 0.05$; **, $p < 0.01$.

3.6: Correlation Between circSKA3 and other Important Genes

Correlation was calculated between all genes to identify potential interaction or regulation of other measured genes with circSKA3, and a correlation matrix was generated with correlation coefficients and p values included in Figure 3.11.

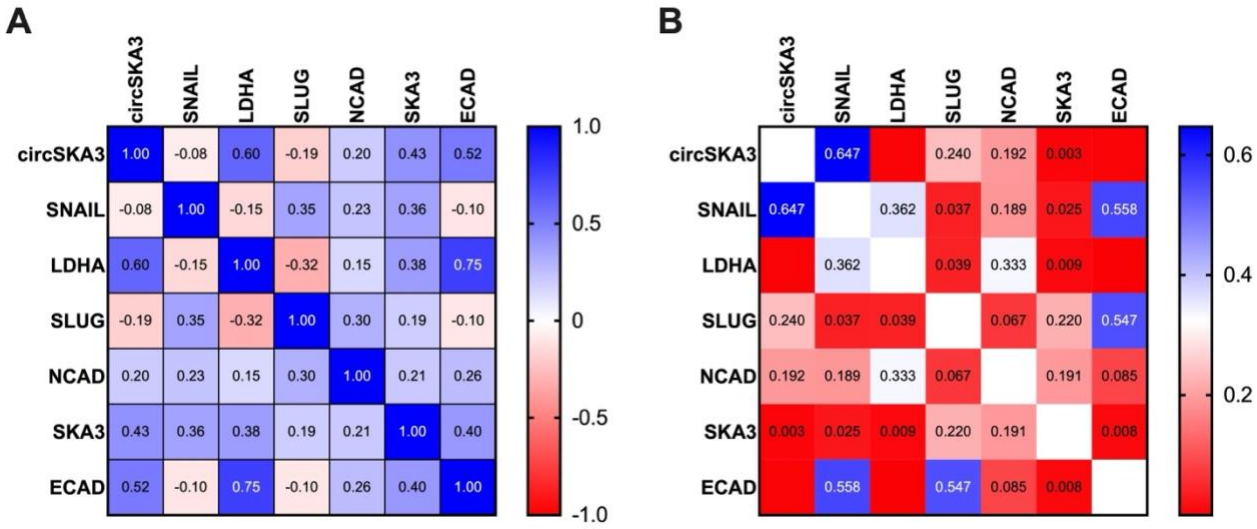

Figure 3.11: Spearman correlation matrix showing the relationship between r and p values for circSKA3 and other measured genes.

A) Non-parametric Spearman correlation coefficient (r) was computed by comparing $2^{-\Delta\Delta ct}$ values for each gene and pair of tissue samples. Weak negative correlations were observed between circSKA3 vs. *SNAIL/SLUG*, *SNAIL* vs. *LDHA/ECAD*, and *SLUG* vs. *LDHA/ECAD*, while other correlations were positive, with LDHA vs. ECAD being the strongest. B) p-values following Spearman correlation test between measured genes. Of these, only correlations between circSKA3/*LDHA*, circSKA3/*SKA3*, circSKA3/*ECAD*, *SNAIL/SLUG*, *LDHA/SKA3*, *LDHA/ECAD* and *SLUG/NCAD* are statistically significant ($p<0.05$). Analysis and graphs were made using GraphPad Prism 10.

Briefly, significant correlations, including circSKA3/*LDHA*, circSKA3/*SKA3*, circSKA3/*ECAD*, *SNAIL/SLUG*, *LDHA/SKA3*, *LDHA/ECAD*, and *SLUG/NCAD*, were observed.

Significant interactions with circSKA3 are plotted and visualized in linear regression in Figure 3.12.

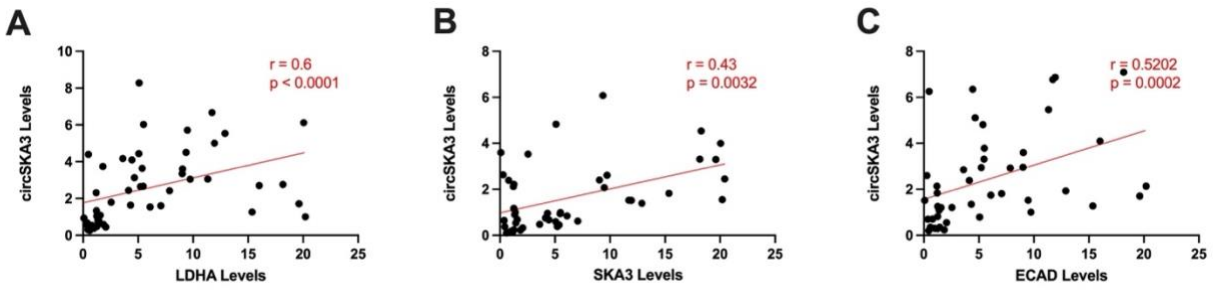

Figure 3.12: Linear regression plots of genes significantly correlated with circSKA3.

A) Correlation between circSKA3 and LDHA ($p < 0.0001$, $r = 0.6$). B) Correlation between circSKA3 and SKA3 ($p = 0.0032$, $r = 0.43$). C) Correlation between circSKA3 and ECAD ($p = 0.0002$, $r = 0.5202$). Results are displayed with corresponding p-values and correlation coefficients.

3.7: Generation of circSKA3 BSJ Probe for Protein Pulldown

Following the validation of circSKA3 overexpression, evaluating its effect on tumorigenic properties, and identifying correlations, a probe with circSKA3 BSJ in four repeating intervals was designed to pulldown and identify interacting proteins. A control probe with four repeating intervals of random sequence was also designed. Following synthesis and extraction of the probe DNA from bacteria cells, the probe sequence was confirmed to match the designed template via Sanger sequencing (Figure 3.13A). Afterward, circSKA3 level was increased by over 100 folds in OVCAR3 cells following transient transfection for 48 hours with circSKA3 overexpression construct and empty vector control to prepare lysates for pulldown (Figure 3.13B). To enable subsequent pulldown steps using streptavidin-biotin interaction, varying biotin concentrations were incorporated using PCR to label the probe sequence and visualized on agarose gel (Figure 3.13C). Following optimum biotin labelling, the probe was cleaned and visualized on a gel to confirm specificity for the ensuing steps (Figure 3.13D).

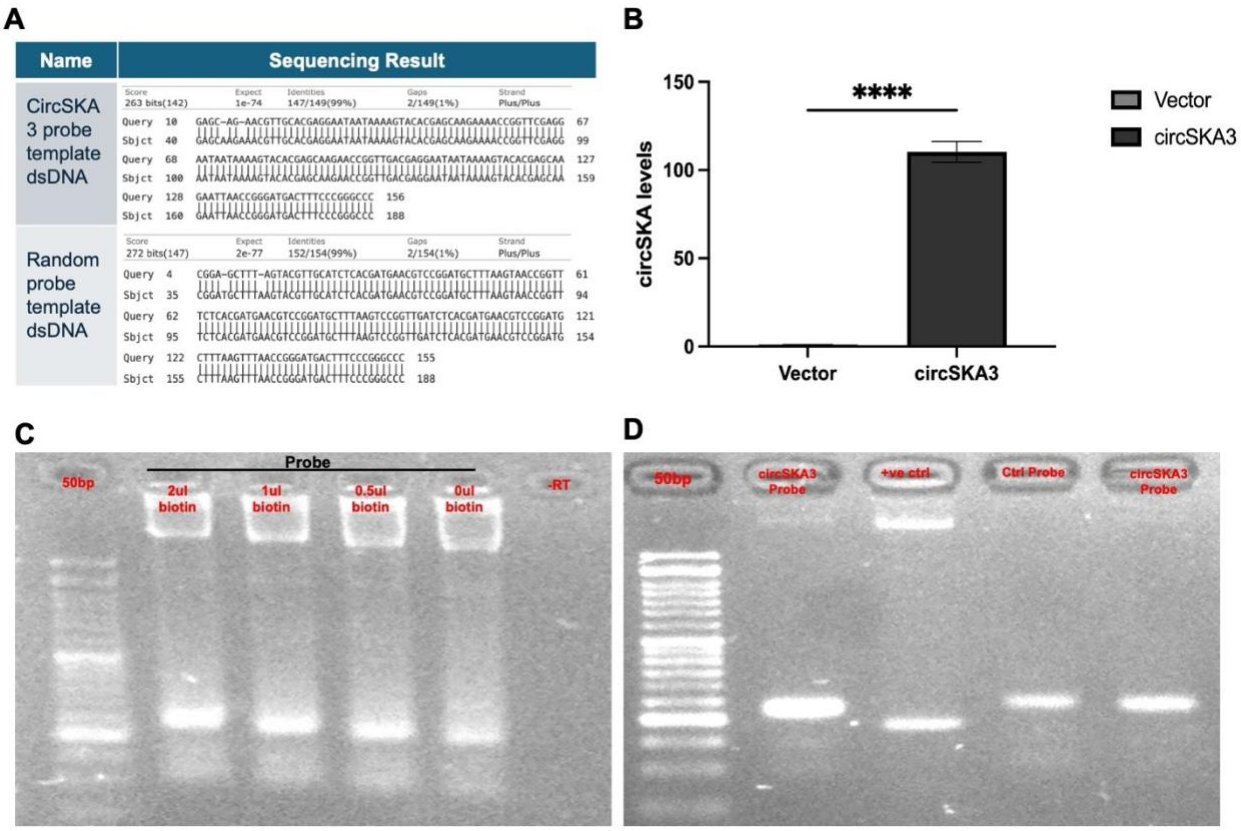

Figure 3.13: Probe design and validation for circSKA3 pulldown assay

A) Sanger sequencing confirms the probe DNA sequence matches the designed template. B) circSKA3 levels increase over 100-fold in OVCAR3 cells following transient transfection with circSKA3 overexpression construct. C) Gel visualization of biotin dCTP-labelled pulldown probes generated using PCR with varying concentrations of biotin dCTP. D) Gel visualization of biotin dCTP-labelled pulldown probes following cleaning of PCR products to remove unspecific products, including unlabelled probe sequences. ****, $p < 0.0001$.

3.8: Proteomic Analysis of circSKA3 Pulldown

After pulling down circSKA3 interacting proteins with the design probes and following stringent washing conditions as defined in the materials and method section, samples were sent for MS. Abundance values of the protein hits were calculated using MSstats Shiny package in R and proteins exclusively expressed in samples pulled down with circSKA3 probe, but not in samples pulled-down pull with control probe, were chosen for further analysis. A heat map below displays the list of proteins and their relative abundance (Figure 3.14).

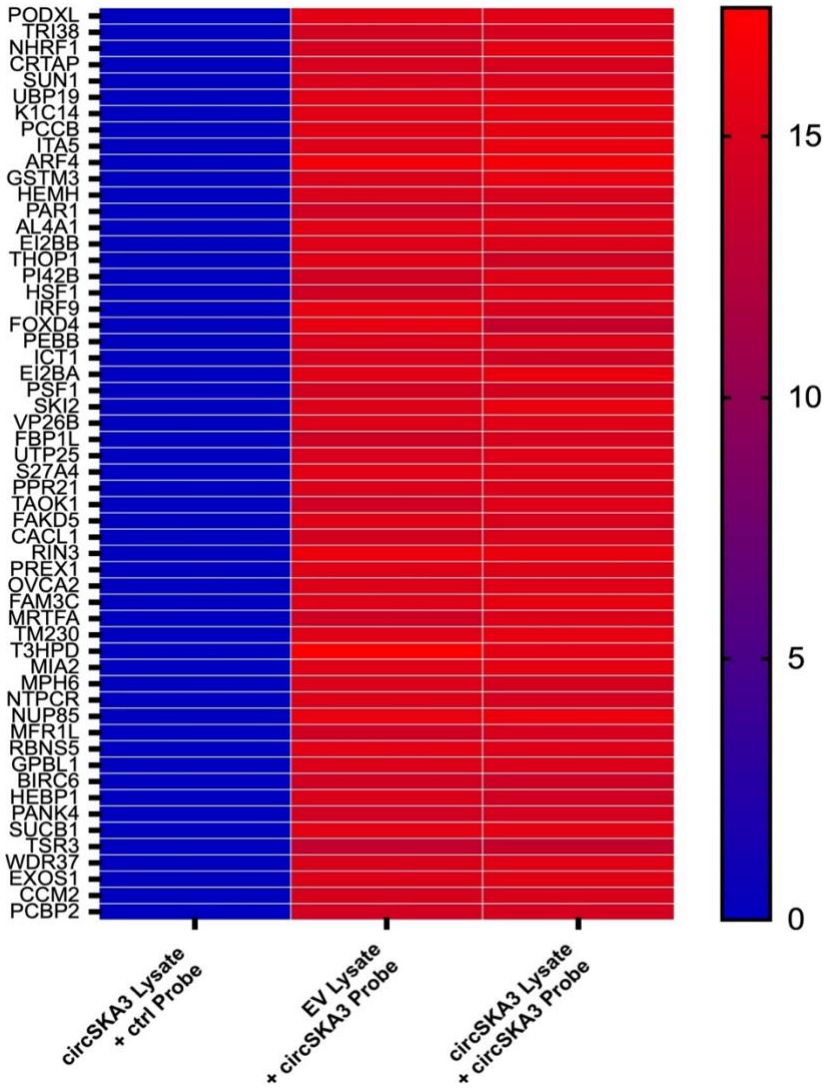

Figure 3.14: Heatmap illustrating the relative abundance of proteins identified in samples pulled down with the circSKA3 probe.

Fifty-seven proteins specifically captured after pulling down with the circSKA3 probe were selected for further analysis and future investigations.

To understand relevant biological processes, molecular functions, cellular components, and pathways regulated by the potential circSKA3 interacting proteins, functional enrichment analysis using ClueGO and CluePedia plug-in in Cytoscape was performed with a minimum Go Tree interval (minimum distance between related terms in GO hierarchy) and a cluster of at least

two and maximum level of 18 proteins interacting together in a network. Major pathways and functions of these proteins are provided in a network diagram below (Figure 3.15). Highlighted processes include morphogenesis of epithelial sheet, ligase activity forming carbon-carbon bonds, nuclear exosomal RNase complex, Hsp90 protein binding function, negative regulation of defense response to virus and arginine, and proline metabolism.

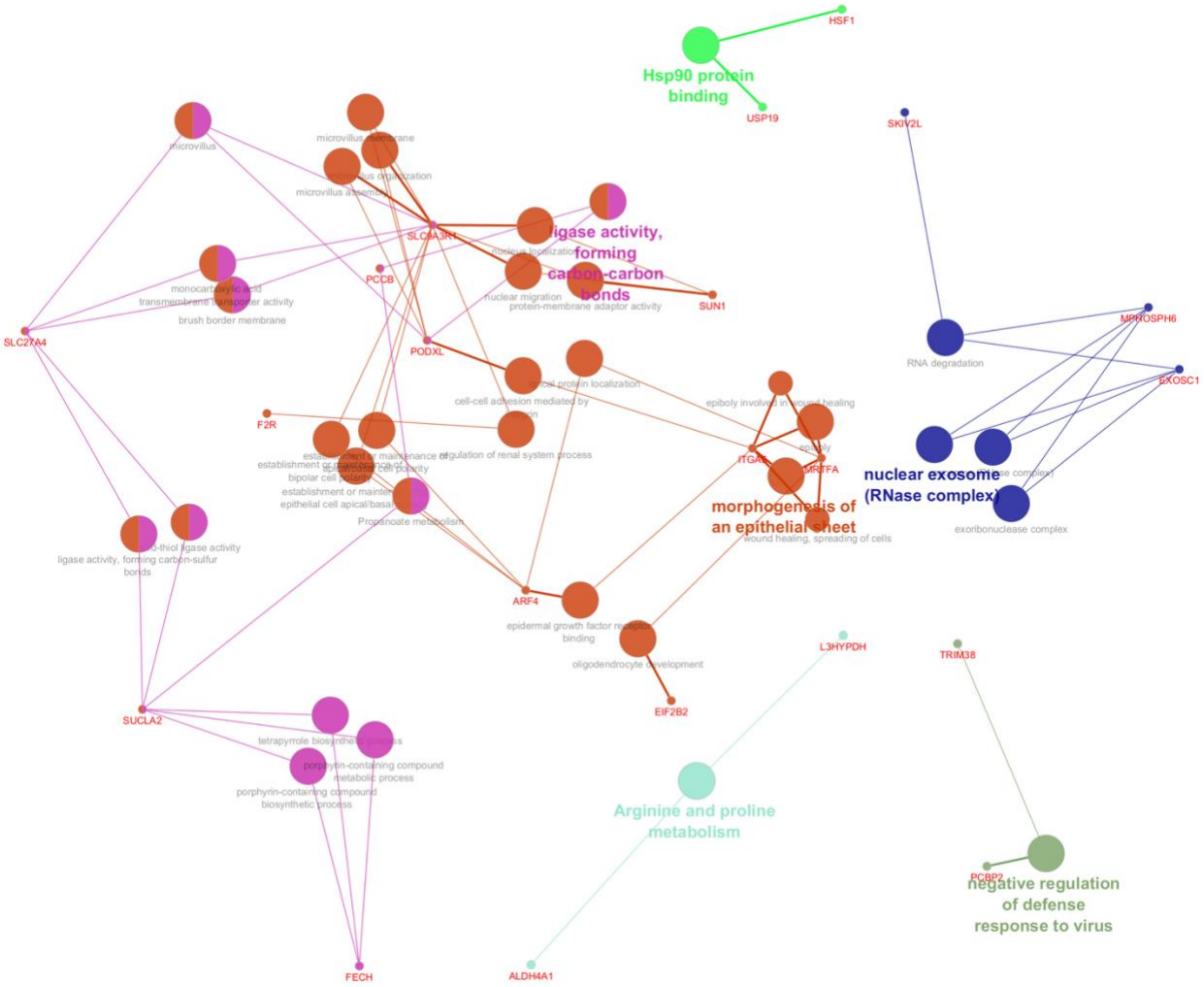

Figure 3.15: Functional analysis of ontology enrichment using ClueGO.

The figure displays a network diagram generated through ontology analysis using ClueGO and CluePedia plug-in in Cytoscape. Major pathways, processes, and functions of the proteins include morphogenesis of epithelial sheet, ligase activity forming carbon-carbon bonds, nuclear exosomal RNase complex, Hsp90 protein binding function, negative regulation of defense response to the virus, and arginine and proline metabolism, ordered by increasing interactions.

Biological processes regulated by these proteins are also displayed in Figure 3.16, with a large percentage participating in signal transduction, cell communication, metabolism, and cell growth and maintenance.

Figure 3.16: Pie chart illustrating an overview of identified biological processes enriched in the potential circSKA3-interacting proteins.

Signal transduction, cell communication, metabolism, energy pathways, cell growth and maintenance, apoptosis and cell adhesion are key processes in order of decreasing percentage composition of the proteins.

Molecular functions are reported and displayed in Figure 3.17, highlighting increased transcription factor activity, transporter activity, ligase activity and receptor signalling complex scaffold activity as major functions of the analyzed proteins.

Figure 3.17: Pie chart illustrating molecular functions enriched in the circSKA3 pulled down protein list.

Transcription factor, transporter, ligase, and receptor signalling complex scaffold activities are the most prominent functions in decreasing order.

3.9: circSKA3-miRNA-mRNA interaction axis prediction

Since a critical mechanism by which circRNAs exert their functions is to sponge miRNAs, leading to upregulation of the target genes of miRNAs, I used bioinformatics tools to identify miRNAs that are predicted to be targeted by circSKA3 (obtained from CircInteractome) and mRNAs that are predicted to be targeted by these miRNAs (obtained from miRDB). From the list of miRNAs predicted to interact with circSKA3, 15 miRNAs with context+score percentile ≥ 90 indicating a very high likelihood of binding to circSKA3 were compiled, and a list of all mRNAs that are predicted to be targeted by each of the miRNAs was combined with that. I then analyzed two whole RNA sequencing data of HGSC and normal ovarian tissues publicly available from SRA following CIRIquant pipeline to estimate gene count using BWA-MEM and HISAT2 alignment. This combined approach allowed a more accurate estimation of RNA counts, and a gene count matrix was generated. Using the DESeq package in R, I identified DEGs and compared them to the compiled list of the 15 miRNAs predicted to interact with circSKA3 and their respective target genes. Following the analysis, nine miRNAs out of the original 15 had at least one DEG compared to the RNAseq analysis (Figure 3.18). The list of genes and miRNA targets were then exported to Cytoscape for network analysis using the source node as the miRNA list and the target node as gene list and presented in Figure 3.19.

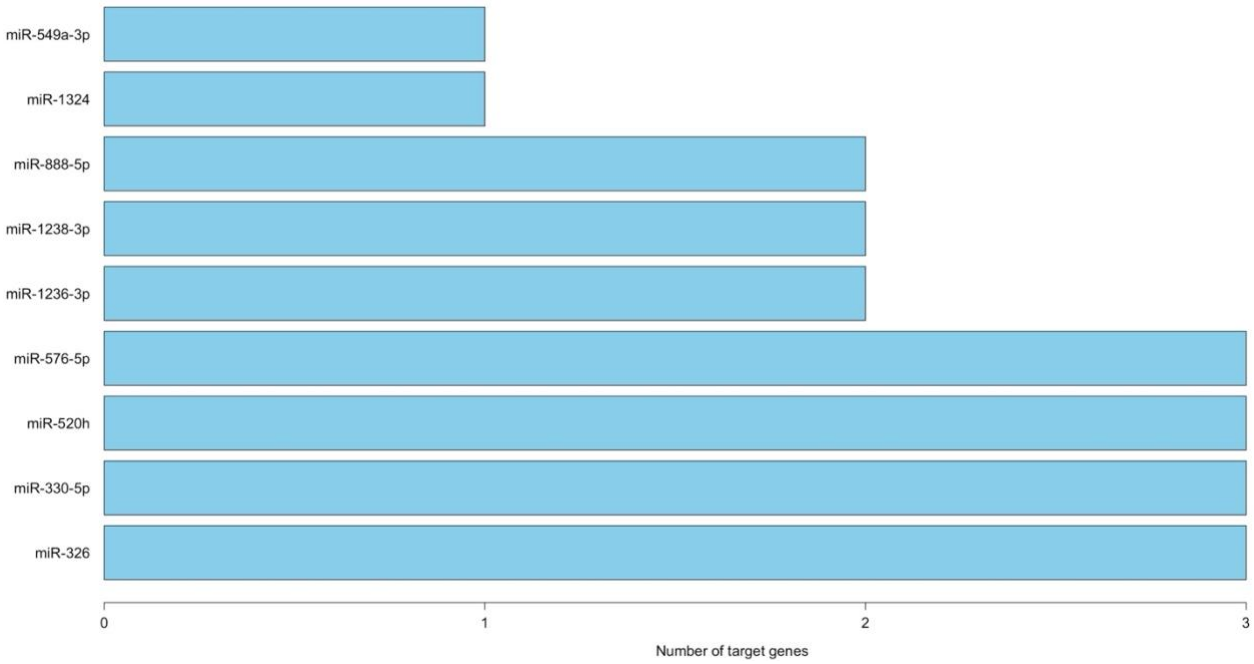

Figure 3.18: List of miRNAs with DEGs in HGSC, including a count of their target genes found to be upregulated in HGSC RNAseq data.

Among the 15 miRNAs predicted to be the targets of circSKA3, 9 miRNAs were identified to have at least one of their predicted target genes upregulated in HGSC compared to the normal ovary in RNAseq datasets analyzed. Hsa-miR-326, 330-5p, and 520h have the network's highest count of target genes (3) upregulated in HGSC.

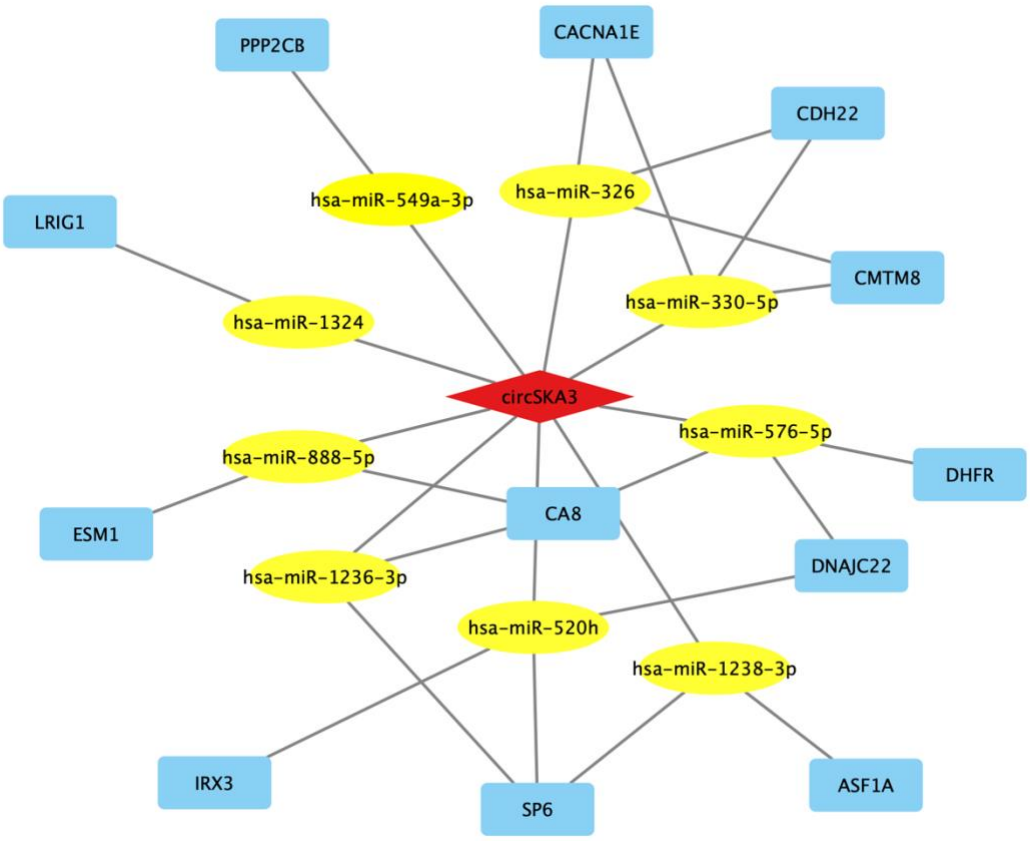

Figure 3.19: Cytoscape network analysis of miRNA-mRNA interactions.

The network analysis was conducted using Cytoscape, where the miRNA list (in yellow ellipse) served as the source nodes and the gene list (in light blue round rectangle) as the target nodes. The resulting network represents the interactions between miRNAs (n=9) and their target genes (n=12) within the circSKA3-miRNA-mRNA interaction axis.

The reported roles of these genes in EOC are summarized below in Table 3.1, with functions ranging from transcription factors to cancer stem cell-promoting pathways. Most of them also contribute to the overall aggressiveness of EOC.

Table 3.1: Target Genes and their functions in the CircSKA3 regulatory network

Reported roles of mRNA predicted to be targeted by miRNAs in the predicted circRNA-miRNA-mRNA network. Most genes have been reported to be abnormally expressed in EOC and impact progression and oncogenicity.

Gene	Reported Role in EOC
CA8	Contributes to GATA family alteration, impacting tumor pathogenesis and prognosis[100].
DHFR	Contributes to chemotherapy resistance and is associated with poor prognosis[101].
DNAJC22	Induced by ARID proteins to promote cancer stem cell phenotype[102].
IRX3	None reported but essential in urogenital system development[103].
SP6	None reported but targets ITGB1 via PI3K/AKT pathway[104].
ASF1A	None reported but prevents senescence via p53 growth arrest in hepatocellular carcinoma (HCC) and prostate cancer cells[105].
ESM1	Upregulated, positively correlated with development and progression via Akt pathway[106].
CDH22	Part of cadherin family with relevance for cancer progression and invasion[107].
CMTM8	Highly expressed and regulates cancerous processes in other tumors[108].
CACNA1E	Promote stem-cell like properties possibly via Akt pathway[109].
PPP2CB	None reported but regulates diverse signalling cascades in cancer cells[110].
LRIG1	Increased expression associated with poor prognosis[111].

Using GO analysis, molecular functions and biological processes to which these 12 genes contribute were also analyzed and presented in Figures 3.20 and 3.21, respectively. Most genes function in signal transduction, cell communication, nucleobase and nucleic acid metabolism regulation, and cell growth/maintenance activities. They perform different activities, including cell adhesion and transcription factor activity.

Figure 3.20: Pie chart illustrating biological processes enriched in predicted miRNA target genes.

Signal transduction, cell communication, and regulation of nucleic acid metabolism are the most prominent functions in decreasing order following GO analysis with FunRich software.

Figure 3.21: Pie chart illustrating molecular functions enriched in predicted miRNA target genes.

Major activities performed by most of the genes in the predicted networks include cell adhesion molecule, transcription factor, catalytic, and chaperone activity.

CHAPTER 4

DISCUSSION

4.1: circSKA3 is Upregulated in HGSC

Aberrant expression of circular RNA has been implicated in different diseases, including cancer, and is increasingly recognized as a modulator of hallmarks of cancer[112]. Most importantly, their differential expression is thought to regulate numerous pathways in the TME, including ECM remodelling, EMT, angiogenesis, and immune response[113]. In EOC, angiogenesis, migration and invasion, and immune evasion are well-characterized hallmarks[114], making circRNA differential expression crucial in tumor development and progression of EOC. As mentioned, circRNAs are spliced from the same mRNA transcript that produces the linear isoforms. A specific increase in circular isoforms of an RNA while conserving the linear RNA expression is thus more interesting as it increasingly suggests a potential role of the circular RNA in that scenario. In this study, I detected a significant increase in the expression level of circSKA3 in HGSC by about five folds compared to LMP and ten folds compared to benign CAF (Figure 1A), while the linear isoform showed no significant difference in HGSC compared to less aggressive tumors (Figure 1B). These results are consistent with findings from circRNA sequencing study from our collaborators (unpublished) and consistent with observations in other tumors, including breast cancer[72], medulloblastoma[78,79,81], glioblastoma[80] and CRC[76,82] where circSKA3 was found to be upregulated in tumors and contributed to increased tumor progression. Together, these findings suggest that upregulation of circSKA3 may be common in different types of cancer, including EOC.

4.2: circSKA3 Exerts Tumor-Promoting Effects in HGSC

Upon discovering the differential expression of circSKA3 and to investigate its potential role in HGSC tumorigenicity, cell lines stably expressing circSKA3 at levels similar to the mean

endogenous expression from HGSC tissue samples and those with circSKA3 knockdown were developed and utilized for functional studies.

Proliferative abilities were observed over seven days with the stable cell lines. I observed no change in proliferative abilities following circSKA3 overexpression by eight folds in the stable cell line. However, a 70% decrease in expression led to reduced proliferative abilities. Previous studies from our lab showed that transient overexpression of circSKA3 up to 250 folds significantly increased proliferative abilities in HGSC cells[91]. Since OVCAR3 cells already expressed high levels of circSKA3, it is possible that an 8-fold increase is not sufficient to produce a significant stimulation of cell proliferation. Significant inhibition of proliferation when endogenous circSKA3 was knocked down, together with our previous findings that strong overexpression of circSKA3 induced cell proliferation, supports a tumor-promoting effect of circSKA3 in HGSC via cell proliferation.

Results from the clonogenic assays highlight the ability of individual HGSC cells to proliferate and form their colonies over an extended period, indicating cellular resistance to death. Positive regulation of this process by circSKA3 reinforces its role in promoting cell growth and survival, thus leading to increased aggressiveness.

Increased migrative abilities indicate passive metastasis in OC and are heavily dependent on cell motility, including actin polymerization and depolymerization pathways[115]. As aforementioned, the *SKA3* gene from which circSKA3 is derived regulates polymerization and depolymerization processes and, as such, could contribute to the increased migrative potentials in HGSC. Studies have also shown increased breast cancer invasiveness due to increased invadopodium formation by circSKA3[72], further confirming the essential role of circSKA3 in this pathway and how this might facilitate increased oncogenicity.

Like other studies, our findings suggest that circSKA3 expression contributes to increased tumor malignancy by promoting tumor growth, metastasis, and invasion[72,76]. Sustained proliferation is a shared characteristic of numerous cancers, including EOC. It is central to carcinogenesis via multiple pathways, including factors related to EMT, TME modification, hypoxia, altered cell metabolism, and signal transduction[116]. As observed from the proliferative assay in this study, circSKA3 increased proliferative abilities, implying the presence of underlying mechanisms that contribute to sustained proliferation. Increased colony-forming abilities, as observed from clonogenic assays, suggest that circSKA3 induces cell survival and might inhibit their senescence by resisting apoptosis, for instance. A similar effect has been noted in medulloblastoma where circSKA3 confined apoptosis to increase tumor migration and invasive abilities[79]. Together, this suggests that circSKA3 might contribute to sustained proliferative abilities in EOC via modulation of cellular apoptosis. This also highlights targeting circSKA3 expression as a promising therapeutic target as it decreases the proliferative, migrative, and clonogenic abilities of HGSC cells and might overcome the challenges of chemotherapy and radiation therapy resistance.

4.3: EMT & Cellular Metabolism are Notable Pathways of circSKA3 Action in HGSC.

To investigate cellular metabolism, the expression level of *LDHA* was measured across the tissue samples. A significant increase in *LDHA* expression was observed in LMP and HGSC compared to benign CAF, suggesting increased *LDHA*-dependent metabolism in HGSC. *LDHA* stands for lactose dehydrogenase A, and its gene encodes the *LDHA* metabolic enzyme, which drives the conversion of pyruvate to lactate, thus reducing pyruvate availability for the citric acid cycle. Numerous studies have confirmed increased expression of *LDHA* in tumors, including

endometrial and gastric cancer, and they contribute to promoting EMT, cellular proliferation, invasion and migration, and cytoskeletal remodelling[117]. As such, increased expression in HGSC was expected and predicted to be linked to other crucial pathways listed earlier. Also significant is the Warburg effect, a metabolic phenomenon in cancer cells driving increased glucose uptake despite an abundance of oxygen and, in turn, facilitating lactate production as the primary source of energy for these cells[118]. Since LDHA plays a key role in the lactate production in this effect, it has also been reported from our lab to be upregulated following miR-383-5p sponging by circSKA3, and together with correlational analysis indicating a strong positive correlation between circSKA3 expression and LDHA levels in OC tumors, I propose that circSKA3 might contribute to HGSC increased oncogenicity by altering cell metabolism.

Due to the central role of EMT in sustained proliferation, migration, invasion, and metastatic abilities of cancer cells, I predicted it as a major pathway with a potential role in circSKA3 driving increased malignancy in HGSC. As such, I measured the expression levels of EMT markers to elucidate their expression patterns and correlations with circSKA3. Results show a significant decrease in the expression levels of *ECAD* in HGSC compared to LMP and CAF. *ECAD* was also significantly downregulated in benign CAF compared to LMP. *SLUG* was significantly downregulated in HGSC compared to LMP and benign CAF. It was also significantly downregulated in LMP compared to CAF. Other EMT markers measured include *NCAD* and *SNAIL*, with no significant difference in expression level between the tumors; however, the mean expression level of *NCAD* was higher in HGSC than in CAF and LMP.

EMT is typically characterized by an increase in *SNAIL* and *SLUG* transcriptional factors driving a decrease in *ECAD* and an increase in *NCAD* expression levels. In this study, I observed that *ECAD* levels were significantly decreased in HGSC, indicating a suppressed epithelial cell

feature, thus disrupting cell-cell communications and cellular polarity and facilitating cell dissemination, all typical of aggressive tumors. However, no significant difference was noted in *NCAD* and S*NAIL* mRNA levels, while *SLUG* mRNA was significantly downregulated in HGSC samples. While these results are surprising and contrary to what was expected, similar findings have been reported for other tumor types. For example, a study on renal cancer carcinoma (RCC) reported a negative correlation between tumor aggressiveness and *SLUG* protein expression level in advanced RCC compared to non-neoplastic renal tissues[119]. The same study found no significant difference in *SNAIL* expression level in RCC compared to control non-neoplastic renal tissues. Furthermore, Leroy and Mostov propose a requirement of *SLUG* for cell survival only and that it is not a requirement for ECAD downregulation, nor is it an inducer of cell movement[120]. This suggests that *ECAD* downregulation in HGSC, while indicative of EMT, might be regulated by alternate mechanisms independent of *SLUG/SNAIL* transcriptional factors. Correlational analysis in this study also indicates a positively significant correlation between circSKA3/*ECAD*, *SNAIL/SLUG*, and *SLUG/NCAD*. While the other two are expected as *SNAIL* and *SLUG* function together as transcriptional regulators and drive *NCAD* upregulation while downregulating *ECAD,* a positive correlation between circSKA3 and *ECAD* was unexpected, as previous results suggest an increase in EMT. However, these findings could be attributed to different effects, including the complex interplay between circSKA3 and interacting genes, compensatory mechanisms in the cell, and feedback loops in the cell. For example, circSKA3 was also found to be positively correlated with *LDHA*, and *LDHA* was positively correlated with *ECAD*. This illustrates how more complex feedback loops and compensatory mechanisms might contribute to the results observed.

While further research is warranted to conclude, these findings indicate circSKA3 might promote malignancy in HGSC through dual mechanisms involving altered cellular metabolism via upregulation of *LDHA*, driving the Warburg effect, and disruption in EMT dynamics, as evidenced by decreased *ECAD* and *SLUG* expression.

4.4: circSKA3 May Interact With Key Proteins to Drive HGSC oncogenicity.

circSKA3 has been reported to interact with proteins from other studies. As such, we investigated the protein binding activity of circSKA3 by pulling down and identifying interacting proteins via MS. Fifty-seven proteins were identified to be only present following circSKA3 pulldown, and their biological process and relevant molecular functions were analyzed. Major processes and functions for which these proteins are enriched include morphogenesis of epithelial sheet, ligase activity forming a carbon-carbon bond, nuclear exosomal RNase complex, Hsp90 protein binding, arginine and proline metabolism, and negative regulation of defense response to virus.

Morphogenesis of epithelial sheets is a well-known biological process during which epithelial cells undergo remodelling into more complex structures, often as a response to physiological changes, and contributes to ECM remodelling and EMT. Furthermore, this process alters the cells' typical proliferative, apoptotic, invasive, and migrative abilities, thus contributing to the development of hallmarks of cancers[121]. As highlighted by Qui *et al*., numerous circRNAs have also been reported to facilitate EMT to increase oncogenicity[24]. Results from functional assays and correlational analysis from ovarian tumors in this study have also provided similar indications of a dependency of circSKA3 on an ECM or EMT pathway. Together with most interacting proteins facilitating epithelial sheet morphology, we can infer that circSKA3

promotes EMT and ECM remodelling to drive sustained proliferative and migrative abilities in HGSC.

Following the pulldown of proteins interacting with circSKA3, an enrichment of those with Carbon-Carbon ligase activity was also observed. Ligase activity forming C-C bonds is a molecular function referring to the catalytic joining of two molecules via C-C linkages coupled with ATP or similar hydrolysis to drive this process. Notably, this contributes mainly to cellular metabolism dysregulation as numerous metabolic enzymes, including those with acetyl-CoA, propionyl-CoA, and pyruvate carboxylase activities, have been reported to have C-C bond ligase activity[122]. While this ligase activity has not been reported in EOC, this corroborates previous findings in our lab of increased cellular metabolism following circSKA3 overexpression as indicated by elevated LDHA levels. These enzymes also contribute to EOC metastasis via increased de novo lipogenesis and the Warburg effect[123]. Furthermore, the role of other ligases, including E3 ubiquitin ligase[124] and DNA ligase IV[125], have been implicated in protein degradation and DNA repair pathways, respectively. A similar ubiquitin ligase has also been reported to be inactivated in breast cancer due to *BRCA1* mutation[126] making it noteworthy as *BRCA1* mutation is a risk factor for EOC. Ultimately, ligase activity regulation is essential in EOC pathogenesis as it supports transforming normal epithelial cells into cancerous cells, contributes to cell proliferation and chemoresistance[124] and alters DNA repair pathways[127]. More specifically, this finding highlights cellular metabolism alteration as a major pathway via which HGSC aggressiveness is increased by circSKA3.

An enrichment of proteins part of the nuclear exosome RNase complex, a highly conserved complex in RNA metabolism pathway regulating degradation within the nucleus, was also observed. circSKA3 is more stable than linear SKA3, and as such, an enrichment of nuclear

exosome RNase complex is thought to modulate and contribute to the increased stability of this circular RNA[128]. Moreover, this could implicate an abundance of circSKA3 in a detectable amount in bodily serum as numerous circRNAs are enriched in exosomes and can be localized to different locations in the cell[129]. Furthermore, the role of the nuclear exosomal RNase complex has also been implicated in EOC to promote proliferation, migration and invasion via the *wnt* pathway[130]. Nuclear exosomal cargos have also been reported to increase these abilities in EOC and promote EMT, thus driving increased oncogenicity[131].

A few proteins also contribute to Hsp90 protein binding, arginine and proline metabolism, and negative regulation of defense response to viruses. The Hsp family of highly conserved chaperone proteins plays a role in multiple tumors, including EOC, and has been reported to promote EOC drug resistance and expression of anti-apoptotic proteins[132]. Arginine and proline metabolism also contribute to synthesizing these amino acids from glutamate, with ALDH4A1 protein involved in this pathway. This further associates the role of *LDHA* in modulating cancer cell metabolism in HGSC via the Warburg effect to increase tumor growth[133]. Negative regulation of defense response to virus suggests a downregulation of the interferon family, decreasing the immune response of the cells[134]. Suppressed immune response is another hallmark of cancer and suggests the possibility of circSKA3 regulating related pathways to drive tumor aggressiveness in HGSC.

Evidence from these protein interactions and their highlighted molecular functions and biological processes suggests circSKA3 plays a multifaceted role in driving tumor aggressiveness in HGSC through a combination of pathways, including immune response and metabolic pathways, possibly centralized via EMT. Further validations are needed to reveal these mechanisms' intricate workings and links.

4.5: circSKA3-miRNA-mRNA Network Prediction

circSKA3-miRNA-mRNA axis was predicted using bioinformatic analysis of publicly available RNAseq data combined with the predicted miRNA list and their target genes to highlight possible miRNA mRNA targets. Nine miRNAs were predicted to be involved in this network, with some confirmed to interact with circSKA3 and others with implications in EOC oncogenicity. miR-326[78], miR-520-h[81] and miR-1238[82] have already been reported to interact with different isoforms of circSKA3and reduce their endogenous expression via sponging to promote the progression of medulloblastoma and CRC via downregulation of their target genes. miR-1236-3p was found to be downregulated in HGSC and to negatively reduce *ZEB1* levels to increase tumor metastasis, possibly via EMT, as an increased expression of NCAD and downregulation of *ECAD* were observed[135]. Also, miR-549a-3p reduced expression has been reported to promote tumor metastasis in RCC via HIF1α and VEGF secretion, indicative of hypoxia, another hallmark of cancer[136]. Reduced expression of most of the miRNAs in this network seems to increase tumor malignancy, implying that their dysregulation via sponging might contribute to HGSC aggressiveness. Following analysis of the biological processes and molecular functions of target genes in this network, pathways contributing to signal transduction, cellular metabolism, cell communication, and cell growth regulation are highlighted. Interestingly, this is similar to pathways enriched from the list of circSKA3 interacting proteins discussed earlier, further highlighting the potential importance of this pathway in driving HGSC malignancy.

To recapitulate, via experiments, analysis, and discussions in this thesis, the results highlight the pivotal role of circSKA3 in promoting the oncogenicity of HGSC by increasing tumor proliferation, migration, and clonogenic potential. Results suggest this occurs through a

complex regulatory interplay of protein and miRNA interactions modulating EMT and cellular metabolism. Further studies targeted at verifying these interactions would confirm the molecular mechanisms underlying circSKA3's oncogenic effects, provide valuable insights into HGSC pathogenesis, define the biomarker potentials of circSKA3, and inform the development of targeted therapies.

CHAPTER 5

FUTURE DIRECTIONS AND CONCLUSIONS

5.1: Future Directions

To continue investigating the role of circSKA3 in HGSC oncogenicity, *in vivo* experiments should also be conducted to determine tumor-formation and aggressiveness of HGSC following circSKA3 overexpression and knockdown. Tumor xenograft models using nude mice should be established via subcutaneous (sc) or intraperitoneal (ip) injection of HGSC stable cell lines with different expression levels of circSKA3[137]. Tumor growth can be examined following sc injection, while metastasis can be evaluated following ip injection. Upon developing these models, tumor characteristics, including tumor size, localization, and response to chemotherapy, could be evaluated *in vivo.*

To further unravel the molecular workings of circSKA3 and identify specific cellular signaling, functional characterization and validation of protein hits from MS should be carried out via IP, followed by western blotting after overexpression and knockdown of circSKA3 levels in cells. Following this, the specific binding motif of circSKA3 to these proteins should be predicted via bioinformatic analysis, followed by *in vitro* testing and validation. Similarly, expression levels of predicted miRNA and their target genes should be measured to validate the proposed interactions. A more detailed network can also be predicted by conducting parallel circRNA, miRNA, and RNA sequencing of HGSC cells with different expression levels of circSKA3. By confirming these interactions, specific signaling pathways can become more evident and carefully investigated to identify the most effective therapeutic targets.

As suggested by the results obtained, the EMT pathway and cellular metabolism alteration are essential for circSKA3's mode of action in promoting HGSC aggressiveness. As such, the expression level of other EMT markers, including *Vimentin*, *Fibronectin* and *Twist*, should be measured in tissue samples. Afterward, rescue experiments increasing *ECAD* levels

should be performed *in vitro* and *in vivo* to determine whether this reduces tumor aggressiveness. Similarly, metabolic reprogramming of cells via nutrient deprivation or inhibition of glycolytic enzymes following circSKA3 overexpression should be performed to validate cellular metabolism involvement. As these assays inhibit glycolysis, they might promote oxidative metabolism to reverse the Warburg effect. If successful in rescuing the tumor-promoting effect of circSKA3 in HGSC cells, this would substantiate the involvement of metabolic pathways in its action.

5.2: Conclusions

In summary, the findings presented and discussed in this thesis provide evidence validating the increased expression of circSKA3 in HGSC and its role in driving oncogenicity. I observed that circSKA3 was increased in HGSC compared to benign CAF and tumors of LMP. Functional studies revealed that circSKA3 promoted HGSC cell proliferative, migrative, invasive, and clonogenic ability. Preliminary results of AP-MS, followed by pathway analyses, revealed the potential interaction of circSKA3 with proteins involved in pathways contributing to HGSC malignancy, including morphogenesis of epithelial sheets, ligase activity forming carbon-carbon bonds, nuclear exosomal RNase complex, Hsp90 protein binding, arginine and proline metabolism, and negative regulation of defense response to viruses. These interactions suggest that circSKA3 may exert its oncogenic effects through a multifaceted mechanism involving immune response and metabolic pathways, possibly centralized via EMT. Additionally, bioinformatic analysis was utilized to predict a circSKA3-miRNA-mRNA network with enriched target genes contributing to similar pathways and processes as observed following protein interaction analysis. Ultimately, this elucidates potential downstream targets and pathways regulated by circSKA3.

Overall, the comprehensive characterization of circSKA3 in HGSC presented in this thesis underscores its significance as a driver of tumor aggressiveness and highlights its potential as both a therapeutic target and a biomarker for distinguishing aggressive tumors from less aggressive ones. Following further research and validations, we can fully understand the detailed and intricate workings underlying circSKA3-mediated oncogenicity in HGSC and translate these findings into clinical applications for improved diagnosis methods and patient outcomes.

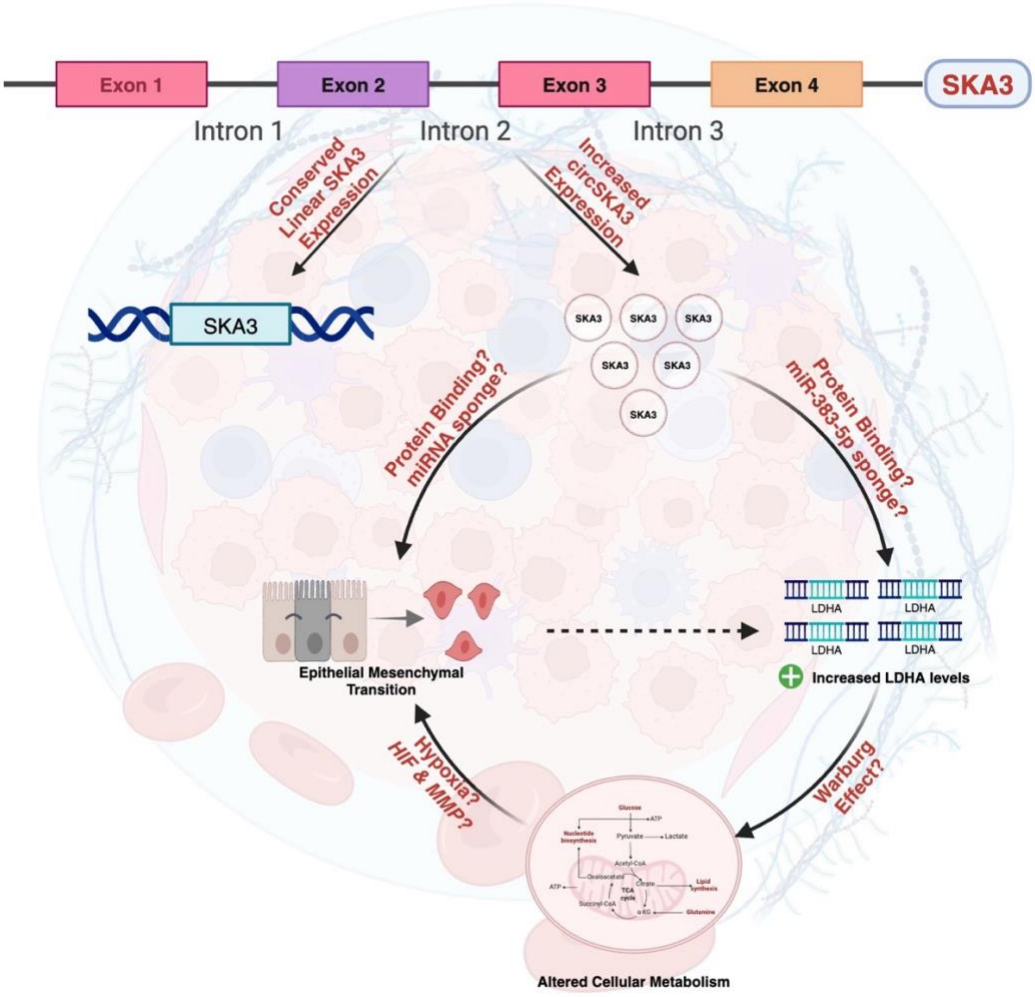

Figure 5.1: Mechanistic illustration of circSKA3 upregulation and its proposed mode of exerting oncogenic effect in HGSC.

circSKA3 might bind proteins and sponge miRNAs to drive increased cellular metabolism and EMT driving tumor aggressiveness in EOC TME.

REFERENCES

1. Sambasivan S. Epithelial ovarian cancer: Review article. *Cancer Treat Res Commun*. 2022;33. doi:10.1016/j.ctarc.2022.100629
2. Meinhold-Heerlein I, Hauptmann S. The heterogeneity of ovarian cancer. *Arch Gynecol Obstet*. 2014;289(2):237-239. doi:10.1007/s00404-013-3114-3
3. Gajjar K, Ogden G, Mujahid MI, Razvi K. Symptoms and Risk Factors of Ovarian Cancer: A Survey in Primary Care. *Obstetrics and Gynecology*. 2012;2012. doi:10.5402/2012/754197
4. Stephanie Lheureux MP, Marsela Braunstein MsP, Amit M. Oza M. Epithelial Ovarian Cancer: Evolution of Management in the Era of Precision Medicine. Published online 2019. doi:10.3322/caac.21559
5. Jones MR, Kamara D, Karlan BY, Pharoah PDP, Gayther SA. Genetic epidemiology of ovarian cancer and prospects for polygenic risk prediction. *Gynecol Oncol*. 2017;147(3):705-713. doi:10.1016/j.ygyno.2017.10.001
6. Torre LA, Trabert B, DeSantis CE, et al. Ovarian cancer statistics, 2018. *CA Cancer J Clin*. 2018;68(4):284-296. doi:10.3322/caac.21456
7. Lisio MA, Fu L, Goyeneche A, Gao ZH, Telleria C. High-Grade Serous Ovarian Cancer: Basic Sciences, Clinical and Therapeutic Standpoints. Published online 2019. doi:10.3390/ijms20040952
8. Kurman RJ, Carcangiu ML, Herrington CS, Young RH. *WHO Classification of Tumours of Female Reproductive Organs (4th Edition)*.; 2014.
9. Cancer Genome Atlas Research Network. Integrated genomic analyses of ovarian carcinoma. *Nature*. 2011;474(7353):609-615. doi:10.1038/nature10166
10. Kannan K, Coarfa C, Rajapakshe K, et al. CDKN2D-WDFY2 is a cancer-specific fusion gene recurrent in high-grade serous ovarian carcinoma. *PLoS Genet*. 2014;10(3):e1004216. doi:10.1371/journal.pgen.1004216
11. Santillan A, Kim YW, Zahurak ML, et al. Differences of chemoresistance assay between invasive micropapillary/low- grade serous ovarian carcinoma and high-grade serous ovarian carcinoma. *International Journal of Gynecological Cancer*. Published online 2007. doi:10.1111/j.1525-1438.2007.00820.x
12. De Leo A, Santini D, Ceccarelli C, et al. What Is New on Ovarian Carcinoma: Integrated Morphologic and Molecular Analysis Following the New 2020 World Health Organization Classification of Female Genital Tumors. *Diagnostics*. 2021;11(4):697. doi:10.3390/diagnostics11040697
13. Dehari R, Kurman RJ, Logani S, Shih IM. *The Development of High-Grade Serous Carcinoma From Atypical Proliferative (Borderline) Serous Tumors and Low-Grade Micropapillary Serous Carcinoma A Morphologic and Molecular Genetic Analysis*.; 2007.

14. Cheasley D, Nigam A, Zethoven M, et al. Genomic analysis of low-grade serous ovarian carcinoma to identify key drivers and therapeutic vulnerabilities. *Journal of Pathology*. 2021;253(1):41-54. doi:10.1002/path.5545
15. Doutel D, Davidson B, Nitschke Pettersen IK, Torgunrud A. Molecular characteristics of low-grade serous carcinoma in effusions. *Cytopathology*. 2023;34(2):99-105. doi:10.1111/cyt.13207
16. Qiu C, Lu N, Wang X, et al. Gene expression profiles of ovarian low-grade serous carcinoma resemble those of fallopian tube epithelium. *Gynecol Oncol*. 2017;147(3):634-641. doi:10.1016/j.ygyno.2017.09.029
17. Leskela S, Romero I, Cristobal E, et al. Mismatch Repair Deficiency in Ovarian Carcinoma: Frequency, Causes, and Consequences. *Am J Surg Pathol*. 2020;44(5):649-656. doi:10.1097/PAS.0000000000001432
18. Murali R, Davidson B, Fadare O, et al. High-grade Endometrial Carcinomas. *International Journal of Gynecological Pathology*. 2019;38:S40-S63. doi:10.1097/PGP.0000000000000491
19. Pierson WE, Peters PN, Chang MT, et al. An integrated molecular profile of endometrioid ovarian cancer. *Gynecol Oncol*. 2020;157(1):55-61. doi:10.1016/j.ygyno.2020.02.011
20. Denschlag D, Ulrich U, Emons G. The diagnosis and treatment of endometrial cancer: progress and controversies. *Dtsch Arztebl Int*. Published online 2010.
21. Del Carmen MG, Birrer M, Schorge JO. Clear cell carcinoma of the ovary: A review of the literature. *Gynecol Oncol*. 2012;126(3):481-490. doi:10.1016/j.ygyno.2012.04.021
22. Iida Y, Okamoto A, Hollis RL, Gourley C, Herrington CS. Clear cell carcinoma of the ovary: A clinical and molecular perspective. *International Journal of Gynecological Cancer*. Published online 2021. doi:10.1136/ijgc-2020-001656
23. Zhu C, Xu Z, Zhang T, et al. Updates of pathogenesis, diagnostic and therapeutic perspectives for ovarian clear cell carcinoma. *J Cancer*. Published online 2021. doi:10.7150/jca.53395
24. Qiu Y, Chen Y, Agbede O, Eshaghi E, Peng C. Circular RNAs in Epithelial Ovarian Cancer: From Biomarkers to Therapeutic Targets. *Cancers 2022, Vol 14, Page 5711*. 2022;14(22):5711. doi:10.3390/CANCERS14225711
25. Morice P, Gouy S, Leary A. Mucinous Ovarian Carcinoma. *New England Journal of Medicine*. 2019;380(13):1256-1266. doi:10.1056/nejmra1813254
26. Webpathology.com: A Collection of Surgical Pathology Images. Accessed May 1, 2024. https://www.webpathology.com/feedback.asp
27. Pectasides D, Pectasides E, Kassanos D. Germ cell tumors of the ovary. *Cancer Treat Rev*. 2008;34(5):427-441. doi:10.1016/j.ctrv.2008.02.002
28. Meinhold-Heerlein I, Fotopoulou C, Harter P, et al. The new WHO classification of ovarian, fallopian tube, and primary peritoneal cancer and its clinical implications. *Arch Gynecol Obstet*. 2016;293(4):695-700. doi:10.1007/s00404-016-4035-8

29. Kaur B. Pathology of malignant ovarian germ cell tumours. *Diagn Histopathol*. 2020;26(6):289-297. doi:10.1016/j.mpdhp.2020.03.006
30. Van Nieuwenhuysen E, Busschaert P, Neven P, et al. The genetic landscape of 87 ovarian germ cell tumors. *Gynecol Oncol*. 2018;151(1):61-68. doi:10.1016/j.ygyno.2018.08.013
31. Schultz KAP, Harris AK, Schneider DT, et al. Ovarian Sex Cord-Stromal Tumors. *J Oncol Pract*. 2016;12(10):940-946. doi:10.1200/JOP.2016.016261
32. Torre LA, Trabert B, DeSantis CE, et al. Ovarian cancer statistics, 2018. *CA Cancer J Clin*. Published online 2018. doi:10.3322/caac.21456
33. Prat J, Belhadj H, Berek J, et al. Figo's staging classification for cancer of the ovary, fallopian tube, and peritoneum: Abridged republication. *J Gynecol Oncol*. Published online 2015. doi:10.3802/jgo.2015.26.2.87
34. Berek JS, Kehoe ST, Kumar L, Friedlander M. Cancer of the ovary, fallopian tube, and peritoneum. *International Journal of Gynecology & Obstetrics*. 2018;143(S2):59-78. doi:10.1002/ijgo.12614
35. Torre LA, Trabert B, DeSantis CE, et al. Ovarian cancer statistics, 2018. *CA Cancer J Clin*. 2018;68(4):284-296. doi:10.3322/caac.21456
36. Zheng H, Tie Y, Wang X, Yang Y, Wei X, Zhao X. Assessment of the diagnostic value of using serum CA125 and GI-RADS system in the evaluation of adnexal masses. *Medicine*. 2019;98(7):e14577. doi:10.1097/MD.0000000000014577
37. Charkhchi P, Cybulski C, Gronwald J, Wong FO, Narod SA, Akbari MR. CA125 and Ovarian Cancer: A Comprehensive Review. *Cancers (Basel)*. 2020;12(12):3730. doi:10.3390/cancers12123730
38. Whitwell HJ, Worthington J, Blyuss O, et al. Improved early detection of ovarian cancer using longitudinal multimarker models. *Br J Cancer*. 2020;122(6):847-856. doi:10.1038/s41416-019-0718-9
39. Anton C, Carvalho FM, Oliveira EI, ArantesRosaMaciel G, Baracat EC, Carvalho JP. A comparison of CA125, HE4, risk ovarian malignancy algorithm (ROMA), and risk malignancy index (RMI) for the classification of ovarian masses. *Clinics*. 2012;67(5):437-441. doi:10.6061/clinics/2012(05)06
40. Chudecka-Głaz AM. ROMA, an algorithm for ovarian cancer. *Clinica Chimica Acta*. 2015;440:143-151. doi:10.1016/j.cca.2014.11.015
41. Liberto JM, Chen SY, Shih IM, Wang TH, Wang TL, Pisanic TR. Current and Emerging Methods for Ovarian Cancer Screening and Diagnostics: A Comprehensive Review. *Cancers (Basel)*. 2022;14(12):2885. doi:10.3390/cancers14122885
42. Fathalla MF. Incessant ovulation and ovarian cancer - a hypothesis re-visited. *Facts Views Vis Obgyn*. 2013;5(4):292-297.
43. Momenimovahed Z, Tiznobaik A, Taheri S, Salehiniya H. Ovarian cancer in the world: epidemiology and risk factors. *Int J Womens Health*. 2019;11:287-299. doi:10.2147/IJWH.S197604

44. Leitzmann MF, Koebnick C, Danforth KN, et al. Body mass index and risk of ovarian cancer. *Cancer*. 2009;115(4):812-822. doi:10.1002/cncr.24086
45. Cottreau C. Physical activity and reduced risk of ovarian cancer. *Obstetrics & Gynecology*. 2000;96(4):609-614. doi:10.1016/S0029-7844(00)00972-8
46. Booth CM, Li G, Zhang-Salomons J, Mackillop WJ. The impact of socioeconomic status on stage of cancer at diagnosis and survival. *Cancer*. 2010;116(17):4160-4167. doi:10.1002/cncr.25427
47. Chang ET, Canchola AJ, Lee VS, et al. Wine and other alcohol consumption and risk of ovarian cancer in the California Teachers Study cohort. *Cancer Causes & Control*. 2007;18(1):91-103. doi:10.1007/s10552-006-0083-x
48. Roett MA, Evans P. Ovarian cancer: An overview. *Am Fam Physician*. Published online 2009.
49. Matulonis UA. Ovarian Cancer. *Hematol Oncol Clin North Am*. Published online 2018. doi:10.1016/j.hoc.2018.09.006
50. Sapiezynski J, Taratula O, Rodriguez-Rodriguez L, Minko T. Precision targeted therapy of ovarian cancer. *Journal of Controlled Release*. Published online 2016. doi:10.1016/j.jconrel.2016.10.014
51. Yang C, Xia BR, Zhang ZC, Zhang YJ, Lou G, Jin WL. Immunotherapy for Ovarian Cancer: Adjuvant, Combination, and Neoadjuvant. *Front Immunol*. Published online 2020. doi:10.3389/fimmu.2020.577869
52. Yang X, Mei J, Wang H, Gu D, Ding J, Liu C. The emerging roles of circular RNAs in ovarian cancer. *Cancer Cell Int*. 2020;20(1):265. doi:10.1186/s12935-020-01367-9
53. Nielsen AF, Bindereif A, Bozzoni I, et al. Best practice standards for circular RNA research. *Nat Methods*. 2022;19(10):1208-1220. doi:10.1038/s41592-022-01487-2
54. Ebbesen KK, Kjems J, Hansen TB. Circular RNAs: Identification, biogenesis and function. *Biochimica et Biophysica Acta (BBA) - Gene Regulatory Mechanisms*. 2016;1859(1):163-168. doi:10.1016/j.bbagrm.2015.07.007
55. He AT, Liu J, Li F, Yang BB. Targeting circular RNAs as a therapeutic approach: current strategies and challenges. *Signal Transduct Target Ther*. 2021;6(1):185. doi:10.1038/s41392-021-00569-5
56. Chen LL, Yang L. Regulation of circRNA biogenesis. *RNA Biol*. 2015;12(4):381-388. doi:10.1080/15476286.2015.1020271
57. Conn SJ, Pillman KA, Toubia J, et al. The RNA Binding Protein Quaking Regulates Formation of circRNAs. *Cell*. 2015;160(6):1125-1134. doi:10.1016/j.cell.2015.02.014
58. Kramer MC, Liang D, Tatomer DC, et al. Combinatorial control of Drosophila circular RNA expression by intronic repeats, hnRNPs, and SR proteins. *Genes Dev*. 2015;29(20):2168-2182. doi:10.1101/gad.270421.115
59. Yu CY, Kuo HC. The emerging roles and functions of circular RNAs and their generation. *J Biomed Sci*. 2019;26(1):29. doi:10.1186/s12929-019-0523-z

60. Zhao X, Cai Y, Xu J. Circular RNAs: Biogenesis, Mechanism, and Function in Human Cancers. *Int J Mol Sci*. 2019;20(16):3926. doi:10.3390/ijms20163926
61. Wang F, Niu Y, Chen K, et al. Extracellular Vesicle–Packaged circATP2B4 Mediates M2 Macrophage Polarization via miR-532-3p/SREBF1 Axis to Promote Epithelial Ovarian Cancer Metastasis. *Cancer Immunol Res*. 2023;11(2):199-216. doi:10.1158/2326-6066.CIR-22-0410
62. Wei W, Wang N, Lin L. Prognostic Value of hsa_circ_0007615 in Epithelial Ovarian Cancer and its Regulatory Effect on Tumor Progression. *Hormone and Metabolic Research*. 2023;55(11):801-808. doi:10.1055/a-2119-3229
63. Lu M, Gong B, Wang Y, Li J. CircBNC2 affects epithelial ovarian cancer progression through the miR-223-3p/LARP4 axis. *Anticancer Drugs*. 2023;34(3):384-394. doi:10.1097/CAD.0000000000001423
64. Chai B, Wu Y, Yang H, et al. Tau Aggregation-Dependent Lipid Peroxide Accumulation Driven by the hsa_circ_0001546/14-3-3/CAMK2D/Tau Complex Inhibits Epithelial Ovarian Cancer Peritoneal Metastasis. *Advanced Science*. Published online April 18, 2024. doi:10.1002/advs.202310134
65. Beilerli A, Begliarzade S, Sufianov A, Ilyasova T, Liang Y, Beylerli O. Circulating ciRS-7 as a potential non-invasive biomarker for epithelial ovarian cancer: An investigative study. *Noncoding RNA Res*. 2022;7(3):197-204. doi:10.1016/j.ncrna.2022.07.004
66. Ning L, Lang J, Long B, Wu L. Diagnostic value of circN4BP2L2 in type I and type II epithelial ovarian cancer. *BMC Cancer*. 2022;22(1):1210. doi:10.1186/s12885-022-10138-w
67. Kramer MC, Liang D, Tatomer DC, et al. Combinatorial control of Drosophila circular RNA expression by intronic repeats, hnRNPs, and SR proteins. *Genes Dev*. 2015;29(20):2168-2182. doi:10.1101/gad.270421.115
68. Chen J, Li Y, Zheng Q, et al. Circular RNA profile identifies circPVT1 as a proliferative factor and prognostic marker in gastric cancer. *Cancer Lett*. 2017;388:208-219. doi:10.1016/j.canlet.2016.12.006
69. Helgeson LA, Zelter A, Riffle M, Maccoss MJ, Asbury CL, Davis TN. Human Ska complex and Ndc80 complex interact to form a load-bearing assembly that strengthens kinetochore-microtubule attachments. 2018;115(11):2740-2745. doi:10.1073/pnas.1718553115
70. Fagerberg L, Hallström BM, Oksvold P, et al. Analysis of the Human Tissue-specific Expression by Genome-wide Integration of Transcriptomics and Antibody-based Proteomics. *Molecular & Cellular Proteomics*. 2014;13(2):397-406. doi:10.1074/mcp.M113.035600
71. Welburn JPI, Grishchuk EL, Backer CB, Wilson-Kubalek EM, Yates JR, Cheeseman IM. The Human Kinetochore Ska1 Complex Facilitates Microtubule Depolymerization-Coupled Motility. *Dev Cell*. 2009;16(3):374-385. doi:10.1016/j.devcel.2009.01.011

72. Du WW, Yang W, Li X, et al. The Circular RNA circSKA3 Binds Integrin β1 to Induce Invadopodium Formation Enhancing Breast Cancer Invasion. *Mol Ther*. 2020;28(5):1287-1298. doi:10.1016/j.ymthe.2020.03.002
73. Du WW, Li X, Ma J, et al. Promotion of tumor progression by exosome transmission of circular RNA circSKA3. *Mol Ther Nucleic Acids*. 2022;27:276-292. doi:10.1016/j.omtn.2021.11.027
74. Xie L, Pan Z. Circular RNA circ_0000467 regulates colorectal cancer development via miR-382-5p/EN2 axis. *Bioengineered*. 2021;12(1):886-897. doi:10.1080/21655979.2021.1889130
75. Song W, Miao L, Zhang K, et al. Sevoflurane suppresses colorectal cancer malignancy by modulating β-catenin ubiquitination degradation via circSKA3. *Cell Signal*. 2024;114:110987. doi:10.1016/j.cellsig.2023.110987
76. Deng J, Liao S, Chen C, et al. Specific intracellular retention of circSKA3 promotes colorectal cancer metastasis by attenuating ubiquitination and degradation of SLUG. *Cell Death Dis*. 2023;14(11):750. doi:10.1038/s41419-023-06279-w
77. Liu J, Chen S, Li Z, Teng W, Ye X. Hsa_circ_0040809 and hsa_circ_0000467 promote colorectal cancer cells progression and construction of a circRNA-miRNA-mRNA network. *Front Genet*. 2022;13. doi:10.3389/fgene.2022.993727
78. Zhao X, Guan J, Luo M. Circ-SKA3 upregulates ID3 expression by decoying miR-326 to accelerate the development of medulloblastoma. *J Clin Neurosci*. 2021;86:87-96. doi:10.1016/j.jocn.2021.01.020
79. Wang X, Xu D, Pei X, et al. Circska3 modulates foxm1 to facilitate cell proliferation, migration, and invasion while confine apoptosis in medulloblastoma via mir-383-5p. *Cancer Manag Res*. Published online 2020. doi:10.2147/CMAR.S272753
80. Zhou M, Li H, Chen K, Ding W, Yang C, Wang X. Circska3 downregulates mir-1 through methylation in glioblastoma to promote cancer cell proliferation. *Cancer Manag Res*. Published online 2021. doi:10.2147/CMAR.S279097
81. Liu XC, Wang FC, Wang JH, Zhao JY, Ye SY. The Circular RNA circSKA3 Facilitates the Malignant Biological Behaviors of Medulloblastoma via miR-520 h/CDK6 Pathway. *Mol Biotechnol*. 2022;64(9):1022-1033. doi:10.1007/s12033-022-00466-4
82. Mao Y, Miao J, Xi L, et al. circSKA3 promotes colorectal cancer metastases through miR-1238 and methylation. *Mol Cell Biochem*. Published online May 31, 2023. doi:10.1007/s11010-023-04773-5
83. Li B, Cai X, Wang Y, et al. Circ-SKA3 Enhances Doxorubicin Toxicity in AC16 Cells Through miR-1303/TLR4 Axis. *Int Heart J*. 2021;62(5):1112-1123. doi:10.1536/ihj.20-809
84. Xu T, Li Y, Zhu N, Su Y, Li J, Ke K. circSKA3 acts as a sponge of miR-6796-5p to be associated with outcomes of ischemic stroke by regulating matrix metalloproteinase 9 expression. *Eur J Neurol*. 2022;29(2):486-495. doi:10.1111/ene.15164

85. O'Brien J, Hayder H, Zayed Y, Peng C. Overview of MicroRNA Biogenesis, Mechanisms of Actions, and Circulation. *Front Endocrinol (Lausanne)*. 2018;9. doi:10.3389/fendo.2018.00402
86. John A, Kubosumi A, Reddy PH. Mitochondrial MicroRNAs in Aging and Neurodegenerative Diseases. *Cells*. 2020;9(6):1345. doi:10.3390/cells9061345
87. Gong L, Zhou X, Sun J. Circular RNAs Interaction with MiRNAs: Emerging Roles in Breast Cancer. *Int J Med Sci*. 2021;18(14):3182-3196. doi:10.7150/ijms.62219
88. Guo L, Jia L, Luo L, et al. Critical Roles of Circular RNA in Tumor Metastasis via Acting as a Sponge of miRNA/isomiR. *Int J Mol Sci*. 2022;23(13):7024. doi:10.3390/ijms23137024
89. Zhu J, Ye J, Zhang L, et al. Differential Expression of Circular RNAs in Glioblastoma Multiforme and Its Correlation with Prognosis. *Transl Oncol*. Published online 2017. doi:10.1016/j.tranon.2016.12.006
90. Lv T, Miao YF, Jin K, et al. Dysregulated circular RNAs in medulloblastoma regulate proliferation and growth of tumor cells via host genes. *Cancer Med*. Published online 2018. doi:10.1002/cam4.1613
91. Esra Eshaghi. *THE INVESTIGATION OF THE SKA3 CIRCULAR RNA ROLE IN THE OVARIAN CANCER PROGRESSION*.; 2022. Accessed May 5, 2024. http://hdl.handle.net/10315/40627
92. Liang D, Wilusz JE. Short intronic repeat sequences facilitate circular RNA production. *Genes Dev*. 2014;28(20):2233-2247. doi:10.1101/gad.251926.114
93. Li F, Wu N, Yang Q, Du WW, Qadir J, Yang BB. Design and use of a back splicing junction probe for pulldown of circular RNA-binding proteins in cell lines. *STAR Protoc*. 2022;3(4). doi:10.1016/j.xpro.2022.101702
94. Lyu M, Li X, Shen Y, et al. CircATRNL1 and circZNF608 Inhibit Ovarian Cancer by Sequestering miR-152-5p and Encoding Protein. *Front Genet*. 2022;13. doi:10.3389/fgene.2022.784089
95. Zhao Q, Laverdure JP, Lanoix J, et al. Proteogenomics Uncovers a Vast Repertoire of Shared Tumor-Specific Antigens in Ovarian Cancer. *Cancer Immunol Res*. 2020;8(4):544-555. doi:10.1158/2326-6066.CIR-19-0541
96. Zhang J, Chen S, Yang J, Zhao F. Accurate quantification of circular RNAs identifies extensive circular isoform switching events. *Nat Commun*. 2020;11(1):90. doi:10.1038/s41467-019-13840-9
97. Love MI, Huber W, Anders S. Moderated estimation of fold change and dispersion for RNA-seq data with DESeq2. *Genome Biol*. 2014;15(12):550. doi:10.1186/s13059-014-0550-8
98. Choi M, Chang CY, Clough T, et al. MSstats: an R package for statistical analysis of quantitative mass spectrometry-based proteomic experiments. *Bioinformatics*. 2014;30(17):2524-2526. doi:10.1093/bioinformatics/btu305

99. Yeung KT, Yang J. Epithelial–mesenchymal transition in tumor metastasis. *Mol Oncol*. 2017;11(1):28-39. doi:10.1002/1878-0261.12017
100. Zhou Q, Yang H jie, Zuo M zhen, Tao Y ling. Distinct expression and prognostic values of GATA transcription factor family in human ovarian cancer. *J Ovarian Res*. 2022;15(1):49. doi:10.1186/s13048-022-00974-6
101. Wang M, Hu T, Xie KY. Dihydrofolate reductase as a predictor for poor response to platinum-based chemotherapy in epithelial ovarian cancer. *Int J Clin Exp Pathol*. 2019;12(5):1723-1730.
102. Dausinas P, Pulakanti K, Rao S, Cole JM, Dahl R, Cowden Dahl KD. ARID3A and ARID3B induce stem promoting pathways in ovarian cancer cells. *Gene*. 2020;738:144458. doi:10.1016/j.gene.2020.144458
103. Fu A, Koth ML, Brown RM, et al. IRX3 and IRX5 collaborate during ovary development and follicle formation to establish responsive granulosa cells in the adult mouse†. *Biol Reprod*. 2020;103(3):620-629. doi:10.1093/biolre/ioaa100
104. Lyu X, Ding X, Ye H, Guo R, Wu M, Cao L. KLF14 targets ITGB1 to inhibit the progression of cervical cancer via the PI3K/AKT signalling pathway. *Discover Oncology*. 2022;13(1):30. doi:10.1007/s12672-022-00494-1
105. Wu Y, Li X, Yu J, Björkholm M, Xu D. ASF1a inhibition induces p53-dependent growth arrest and senescence of cancer cells. *Cell Death Dis*. 2019;10(2):76. doi:10.1038/s41419-019-1357-z
106. Li Y kun, Zeng T, Guan Y, et al. Validation of ESM1 Related to Ovarian Cancer and the Biological Function and Prognostic Significance. *Int J Biol Sci*. 2023;19(1):258-280. doi:10.7150/ijbs.66839
107. Zeller C, Dai W, Curry E, et al. The DNA Methylomes of Serous Borderline Tumors Reveal Subgroups With Malignant- or Benign-Like Profiles. *Am J Pathol*. 2013;182(3):668-677. doi:10.1016/j.ajpath.2012.11.040
108. Zhang M, Wang J, Yue H, Zhang L. Identification of prognostic biomarkers in the CMTM family genes of human ovarian cancer through bioinformatics analysis and experimental verification. *Front Genet*. 2022;13. doi:10.3389/fgene.2022.918319
109. Lee H, Kim JW, Kim DK, et al. Calcium Channels as Novel Therapeutic Targets for Ovarian Cancer Stem Cells. *Int J Mol Sci*. 2020;21(7):2327. doi:10.3390/ijms21072327
110. Ruvolo PP. The broken "Off" switch in cancer signaling: PP2A as a regulator of tumorigenesis, drug resistance, and immune surveillance. *BBA Clin*. 2016;6:87-99. doi:10.1016/j.bbacli.2016.08.002
111. de Melo ALL, Linder A, Sundfeldt K, Lindquist D, Hedman H. Single-molecule array assay reveals the prognostic impact of plasma LRIG1 in ovarian carcinoma. *Acta Oncol (Madr)*. 2022;61(11):1425-1433. doi:10.1080/0284186X.2022.2140016
112. Liu J, Li D, Luo H, Zhu X. Circular RNAs: The star molecules in cancer. *Mol Aspects Med*. 2019;70:141-152. doi:10.1016/j.mam.2019.10.006

113. Song H, Liu Q, Liao Q. Circular RNA and tumor microenvironment. *Cancer Cell Int*. 2020;20(1):211. doi:10.1186/s12935-020-01301-z
114. Heredia-Soto V, López-Guerrero JA, Redondo A, Mendiola M. The hallmarks of ovarian cancer: Focus on angiogenesis and micro-environment and new models for their characterisation. *European Journal of Cancer Supplements*. 2020;15:49-55. doi:10.1016/j.ejcsup.2019.11.003
115. Yeung TL, Leung CS, Yip KP, Au Yeung CL, Wong STC, Mok SC. Cellular and molecular processes in ovarian cancer metastasis. A Review in the Theme: Cell and Molecular Processes in Cancer Metastasis. *American Journal of Physiology-Cell Physiology*. 2015;309(7):C444-C456. doi:10.1152/ajpcell.00188.2015
116. Feitelson MA, Arzumanyan A, Kulathinal RJ, et al. Sustained proliferation in cancer: Mechanisms and novel therapeutic targets. *Semin Cancer Biol*. 2015;35 Suppl(Suppl):S25-S54. doi:10.1016/j.semcancer.2015.02.006
117. Mishra D, Banerjee D. Lactate Dehydrogenases as Metabolic Links between Tumor and Stroma in the Tumor Microenvironment. *Cancers (Basel)*. 2019;11(6). doi:10.3390/cancers11060750
118. Tondo-Steele K, McLean K. The "Sweet Spot" of Targeting Tumor Metabolism in Ovarian Cancers. *Cancers (Basel)*. 2022;14(19). doi:10.3390/cancers14194696
119. Mikami S, Katsube KI, Oya M, et al. Expression of Snail and Slug in renal cell carcinoma: E-cadherin repressor Snail is associated with cancer invasion and prognosis. *Laboratory Investigation*. 2011;91(10):1443-1458. doi:10.1038/labinvest.2011.111
120. Leroy P, Mostov KE. Slug is required for cell survival during partial epithelial-mesenchymal transition of HGF-induced tubulogenesis. *Mol Biol Cell*. 2007;18(5):1943-1952. doi:10.1091/mbc.e06-09-0823
121. Wang CC, Jamal L, Janes KA. Normal morphogenesis of epithelial tissues and progression of epithelial tumors. *Wiley Interdiscip Rev Syst Biol Med*. 2012;4(1):51-78. doi:10.1002/wsbm.159
122. The Gene Ontology Resource: 20 years and still GOing strong. *Nucleic Acids Res*. 2019;47(D1):D330-D338. doi:10.1093/nar/gky1055
123. Wang M, Zhang J, Wu Y. Tumor metabolism rewiring in epithelial ovarian cancer. *J Ovarian Res*. 2023;16(1):108. doi:10.1186/s13048-023-01196-0
124. Meng Y, Qiu L, Zhang S, Han J. The emerging roles of E3 ubiquitin ligases in ovarian cancer chemoresistance. *Cancer Drug Resist*. 2021;4(2):365-381. doi:10.20517/cdr.2020.115
125. Assis J, Pereira D, Medeiros R. Ovarian cancer and DNA repair: DNA ligase IV as a potential key. *World J Clin Oncol*. 2013;4(1):14-24. doi:10.5306/wjco.v4.i1.14
126. Hashizume R, Fukuda M, Maeda I, et al. The RING Heterodimer BRCA1-BARD1 Is a Ubiquitin Ligase Inactivated by a Breast Cancer-derived Mutation. *Journal of Biological Chemistry*. 2001;276(18):14537-14540. doi:10.1074/jbc.C000881200

127. Kao SH, Wu HT, Wu KJ. Ubiquitination by HUWE1 in tumorigenesis and beyond. *J Biomed Sci*. 2018;25(1):67. doi:10.1186/s12929-018-0470-0
128. Ren L, Jiang Q, Mo L, et al. Mechanisms of circular RNA degradation. *Commun Biol*. 2022;5(1):1355. doi:10.1038/s42003-022-04262-3
129. Han Z, Chen H, Guo Z, et al. Circular RNAs and Their Role in Exosomes. *Front Oncol*. 2022;12:848341. doi:10.3389/fonc.2022.848341
130. Nakamura K, Sawada K, Kobayashi M, et al. Role of the Exosome in Ovarian Cancer Progression and Its Potential as a Therapeutic Target. *Cancers (Basel)*. 2019;11(8). doi:10.3390/cancers11081147
131. Enriquez VA, Cleys ER, Da Silveira JC, Spillman MA, Winger QA, Bouma GJ. High LIN28A Expressing Ovarian Cancer Cells Secrete Exosomes That Induce Invasion and Migration in HEK293 Cells. *Biomed Res Int*. 2015;2015:1-13. doi:10.1155/2015/701390
132. Yin L, Yang Y, Zhu W, et al. Heat Shock Protein 90 Triggers Multi-Drug Resistance of Ovarian Cancer via AKT/GSK3β/β-Catenin Signaling. *Front Oncol*. 2021;11:620907. doi:10.3389/fonc.2021.620907
133. Liu W, Hancock CN, Fischer JW, Harman M, Phang JM. Proline biosynthesis augments tumor cell growth and aerobic glycolysis: involvement of pyridine nucleotides. *Sci Rep*. 2015;5(1):17206. doi:10.1038/srep17206
134. Macpherson AM, Barry SC, Ricciardelli C, Oehler MK. Epithelial Ovarian Cancer and the Immune System: Biology, Interactions, Challenges and Potential Advances for Immunotherapy. *J Clin Med*. 2020;9(9):2967. doi:10.3390/jcm9092967
135. WANG Y, YAN S, LIU X, et al. miR-1236-3p represses the cell migration and invasion abilities by targeting ZEB1 in high-grade serous ovarian carcinoma. *Oncol Rep*. 2014;31(4):1905-1910. doi:10.3892/or.2014.3046
136. Xuan Z, Chen C, Tang W, et al. TKI-Resistant Renal Cancer Secretes Low-Level Exosomal miR-549a to Induce Vascular Permeability and Angiogenesis to Promote Tumor Metastasis. *Front Cell Dev Biol*. 2021;9:689947. doi:10.3389/fcell.2021.689947
137. Karakashev S, Zhang RG. Mouse models of epithelial ovarian cancer for preclinical studies. *Zool Res*. 2021;42(2):153-160. doi:10.24272/j.issn.2095-8137.2020.382

APPENDICES

Appendix A

Table A.1: List and sequences of primers used for qPCR and PCR.

Primers	Sequences
18s rRNA (qPCR)	5’ GGCGCCCCCTCGATGCTCTTAG 3’ 5’ GCTCGGGCCTGCTTTGAACACTCT 3'
circSKA3 (qPCR)	5’ CACAATGGGACTTAAAAATGCGAG 3’ 5’ CACAATTAGACAACTCTGGGTCAG 3’
ECAD (qPCR)	5’ GCCAAGCAGCAGTACATTCTACACG 3’ 5’ GCTGTTCTTCACGTGCTCAAAATCC 3’
GAPDH (qPCR)	5’ CATGGCAAATTCCATGGCAC 3’ 5’ CACTTGATTTTGGAGGGATC 3’
LDHA (qPCR)	5’ CACCAAAGATTGTCTCTGGCA 3’ 5’ AAGATGTTCACGTTACGCTGG 3’
MUC16 (qPCR)	5’ GATGTCAAGCCAGGCAGCACAA 3’ 5’ GAGAGTGGTAGACATTTCTGGGC 3’
NCAD (qPCR)	5’ AGCAAGCCGCTCTACACCAT 3’ 5’ TGCGCAGTGCTTTCTCTGTC 3’
SKA3 (qPCR)	5’ TACACGAGCAAGAAGCCATTA 3’ 5’ CCTCGCATTTTTAAGTCCCAT 3’
SKA3 + RE site (5’ EcorV --- SacII 3’)	5’ CCGGATATCTACACGAGCAAGAAGCCATTA 3’ 5’ TCCCCGCGGCTTTTATTATTCCTCGCATTT 3’
Slug (qPCR)	5’ ATGAGGAATCTGGCTGCTGT 3’ 5’ CAGGAGAAAATGCCTTTGGA 3’
SNAIL (qPCR)	5’ CCTCCCTGTCAGATGAGGAC 3’ 5’ CCAGGCTGAGGTATTCCTTG 3’
CircSKA3 pulldown probe	5’ CAGCTCAGAGTGTCTTTG 5’ GGGCCCGGGAAAGTCATC
Random pulldown probe	5’ CAGCTCAGAGTGTCTTTG 5’ GGGCCCGGGAAAGTCATC

Table A.2: Sequences of probes used for circSKA3 BSJ pulldown.

Probes consist of four repeating units of circSKA3 BSJ or random sequence flanked by spacers and primer sequence.

Name	Probe Sequence
CircSKA3 probe template dsDNA	5’ CAGCTCAGAGTGTCTTTG CGAGGAATAATAAAAGTACACGAGCAAGAA **ACGTTGCA** CGAGGAATAATAAAAGTACACGAGCAAGAA **AACCGGTT** CGAGGAATAATAAAAGTACACGAGCAAGAA **CCGGTTGA** CGAGGAATAATAAAAGTACACGAGCAAGAA **TTAACCGG** GATGACTTTCCCGGGCCC 3’
Random probe template dsDNA	5’ CAGCTCAGAGTGTCTTTG TCTCACGATGAACGTCCGGATGCTTTAAGT **ACGTTGCA** TCTCACGATGAACGTCCGGATGCTTTAAGT **AACCGGTT** TCTCACGATGAACGTCCGGATGCTTTAAGT **CCGGTTGA** TCTCACGATGAACGTCCGGATGCTTTAAGT **TTAACCGG** GATGACTTTCCCGGGCCC 3’

Table A.3: Sequences cloned into shRNA construct targeting circSKA3 BSJ sequence.

Name	Probe Sequence
shCircSKA3	GAGGAATAATAAAAGTACA
Negative Ctrl	TTCTCCGAACGTGTCACGAT

Table A.4: Description and tumor bank number of clinical samples used in this project.

Tumor Bank #	Description	Tumor Bank #	Description	Tumor Bank #	Description
806	LMP Serous	**1481**	LMP Serous	**2174**	Serous HG
852	Cystadenoma (serous)	**1500**	Cystadenoma (serous)	**2183**	Serous HG
862	LMP Serous	**1535**	LMP Serous	**2184**	Serous HG
896	LMP Serous	**1538**	Cystadenoma (serous)	**2185**	Serous HG
907	Cystadenofibroma (serous)	**1565**	LMP Serous	**2193**	Serous HG
929	LMP Serous	**1716**	LMP Serous	**2210**	Serous HG
942	LMP Serous	**1731**	LMP Serous	**2220**	Serous HG
980	LMP Serous	**1752**	LMP Serous	**2232**	Serous HG
1187	Cystadenofibroma (serous)	**1765**	LMP Serous	**2233**	Serous HG
1220	LMP Serous	**1768**	LMP Serous	**2235**	Serous HG
1267	Cystadenoma (serous)	**1797**	LMP Serous	**2242**	Serous HG
1293	Cystadenoma (serous)	**2033**	Cystadenofibroma (serous)	**2269**	Serous HG
1333	LMP Serous	**2088**	Cystadenofibroma (serous)	**2286**	Serous HG
1383	Cystadenofibroma (serous)	**2110**	LMP Serous	**2289**	Serous HG
1430	LMP Serous	**2118**	Serous HG	**2290**	Serous HG
1449	Cystadenofibroma (serous)	**2126**	Serous HG	**2299**	Serous HG
1453	LMP Serous	**2129**	Serous HG	**2313**	Serous HG
1455	Cystadenofibroma (serous)	**2146**	Cystadenofibroma (serous)	**2321**	Serous HG
1460	Cystadenofibroma (serous)	**2153**	Cystadenoma (serous)	**2322**	Serous HG
1468	LMP Serous	**2157**	Serous HG	**2326**	Serous HG